The Astrophysical Journal, 660:1556–1571, 2007 May 10

CHARACTERIZATION OF DUSTY DEBRIS DISKS: THE *IRAS* AND *HIPPARCOS* CATALOGS

Joseph H. Rhee,[1] Inseok Song,[1] B. Zuckerman,[2] and Michael McElwain[2]
Received 2006 June 6; accepted 2006 September 19

ABSTRACT

Dusty debris disks around main-sequence stars are signposts for the existence of planetesimals and exoplanets. From cross-correlating *Hipparcos* stars with the *IRAS* catalogs, we identify 146 stars within 120 pc of Earth that show excess emission at 60 μm. This search took special precautions to avoid false positives. Our sample is reasonably well distributed from late B to early K-type stars, but it contains very few later type stars. Even though *IRAS* flew more than 20 years ago and many astronomers have cross-correlated its catalogs with stellar catalogs, we were still able to newly identify debris disks at as many as 33 main-sequence stars; of these, 32 are within 100 pc of Earth. The power of an all-sky survey satellite like *IRAS* is evident when comparing our 33 new debris disks with the total of only 22 dusty debris disk stars first detected with the more sensitive, but pointed, satellite *ISO*. Our investigation focuses on the mass, dimensions, and evolution of dusty debris disks.

Subject headings: infrared: stars — planetary systems: protoplanetary disks

Online material: color extended figure set, machine-readable table

1. INTRODUCTION

Dusty debris disks that surround nearby main-sequence stars were first detected by the *Infrared Astronomical Satellite* (*IRAS*) in 1983. These circumstellar disks were inferred from an infrared excess flux between 25 and 100 μm many times brighter than expected from the stellar photosphere. The IR excess was modeled by disk distributions that would absorb optical and ultraviolet flux from the host star and then isotropically radiate this energy at the IR. The first dusty debris disk was discovered around the bright main-sequence star Vega (Aumann et al. 1984); consequently a dusty disk around a main-sequence star is commonly referred to as the Vega phenomenon.

Numerous studies of T Tauri stars dating back many years indicate the characteristic timescale for the dispersal of a surrounding dusty, gaseous disk is a few million years. Following dissipation of the gaseous component, the remaining dust can further dissipate during the following few million years via coagulation into large objects, Poynting-Robertson and stellar wind drag, radiation pressure, and collisional destruction (e.g., Backman & Paresce 1993; Lagrange et al. 2000; Dominik & Decin 2003; Plavchan et al. 2005). Vega-like stars are, however, generally much older than 10 Myr; thus, the observed dust should be of secondary origin, most likely replenished via collision and fragmentation of planetesimals. Furthermore, the Vega phenomenon overlaps with the important planetary system formation epochs in our solar system: giant gas planet formation within ~10 Myr, terrestrial planet formation within ~30 Myr, and the era of heavy bombardment in the inner solar system within ~600 Myr. Therefore, studies of IR-excess stars can provide crucial information on extrasolar planetary formation and evolution.

During the past two decades, about two dozen papers have been published that describe *IRAS*, *Infrared Space Observatory* (*ISO*), and *Spitzer Space Telescope* searches for stars with excess IR emission (§ 3; Lagrange et al. 2000; Zuckerman 2001; Decin et al. 2003). These searches employed different techniques for cross-correlating IR and stellar sources with no consistent definition of an IR excess. To date, several hundred main-sequence IR-excess stars have been reported in the literature including those that have an IR excess at 25 μm.

A major goal of debris disk research has been to characterize the temporal evolution of the quantity of dust present in the disks. Notwithstanding almost two decades of debris disk research using data from three IR satellites, a convincing assessment of this temporal evolution remains incomplete. Such an assessment requires a large sample of stars and a reliable estimate of the dust mass and the age for each debris disk system. False-positive IR-excess stars due to the large beam size of *IRAS*, and improper search or calibration techniques have contaminated some previous studies. Such contamination of the debris disk population has not only plagued many follow-up observations from ground and/or space observatories but also precludes a global assessment of the distribution and evolution of the dust population.

If the IR excess is from a bona fide dust disk, then the best estimator of dust mass comes from submillimeter flux. Unfortunately, submillimeter flux measurements are difficult, time-intensive observations. A more readily accessible observable is τ, the ratio of excess infrared luminosity due to dust divided by the total energy output from a star. We compute values of τ for each of the IR-excess stars presented in this paper. In § 5.1 we discuss the relationship between submillimeter flux and τ for those Vega-like stars for which both are known, and we derive our own relationship, which is used to predict a dust mass if both τ and the dust disk radius are known.

Furthermore, estimation of stellar age is often troublesome since most nearby IR-excess stars are isolated field stars. In order to obviate the shortcoming of stellar age estimation, several groups are using *Spitzer* to search for IR-excess stars in nearby young stellar groups with well-determined ages (e.g., Stauffer et al. 2005). However, because the distance to all rich clusters is substantial (except for the Hyades), it remains difficult to obtain statistically significant results even with *Spitzer* (Stauffer et al. 2005). Thus, the large, clean sample of relatively nearby field stars we discuss in the present paper can contribute in a

[1] Gemini Observatory, Hilo, HI 96720; jrhee@gemini.edu, song@gemini.edu.
[2] Department of Physics and Astronomy, and NASA Astrobiology Institute, University of California, Los Angeles, CA 90095; ben@astro.ucla.edu, mcelwain@astro.ucla.edu.

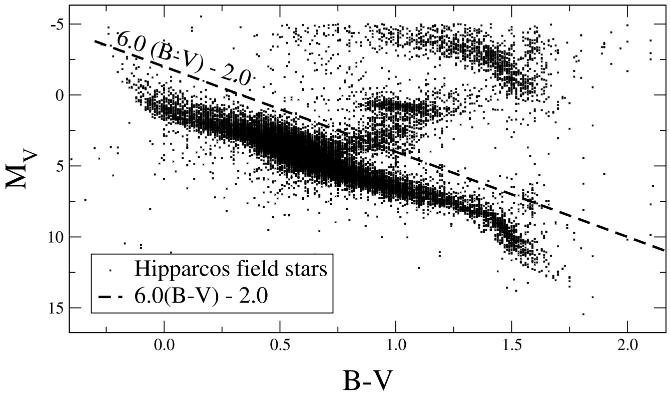

FIG. 1.—H-R diagram of *Hipparcos* field stars. Stars below the dashed line and with $B - V < -0.15$ have been searched for *IRAS* 60 μm excess emission.

statistically meaningful way to our understanding of the Vega phenomenon and its evolution with time.

2. SEARCH CRITERIA AND SELECTION TECHNIQUE

Zuckerman & Song (2004a, hereafter Paper I), relying primarily on data in Silverstone's (2000) thesis, analyzed 58 strong IR excess stars following careful checks against possible contamination from various sources. Zuckerman & Song argued that the Vega-like stars are signposts for the existence of planets and focused their efforts on identifying stars that would make the best targets for adaptive optics and precision radial velocity searches. The present paper extends the sample analyzed in Paper I in several ways. First, we significantly increase the sample size so that it is now possible to address circumstellar dusty disk evolution in a statistically meaningful way. This increase is achieved by systematically cross-correlating all *Hipparcos* main-sequence stars with 60 μm *IRAS* sources in the Faint Source (FSC) and Point Source (PSC) catalogs. Our distance limit is 120 pc compared with the 100 pc adopted in Paper I. Second, the spectral energy distribution (SED) fitting routine was enhanced with the employment of filter response functions and a fully automated fit with a χ^2 minimization method.

Hipparcos and *IRAS* data were cross-correlated to search for IR-excess stars. Many sources in the FSC and PSC with optical stellar identifications are, however, giant stars (Odenwald 1986; Zuckerman et al. 1995b). A constraint on the absolute visual magnitude $M_V \geq 6.0(B - V) - 2.0$ (Fig. 1) was applied to the entire 118,218 stars of the *Hipparcos* catalog to remove giant stars from our sample. This cut eliminated 50,164 stars, leaving 68,054 *Hipparcos* stars for further investigation.

These prescreened *Hipparcos* dwarfs were then cross-correlated against *IRAS* sources. The *IRAS* FSC was used to cross-correlate the 53,157 stars located out of the Galactic plane ($|b| > 10°$), while the PSC was used for the 14,897 stars in the Galactic plane and to recover any object missed by the FSC out of the Galactic plane. All FSC sources with a detection at 60 μm (i.e., a 60 μm flux quality of 2 or 3) and a *Hipparcos* dwarf within 45″ were selected for further investigation. A search radius of 45″ was adopted to reflect the average FSC 3 σ positional error. For PSC sources in the Galactic plane, *Hipparcos* dwarfs within only a 10″ search radius were retained, in order to avoid contamination of spurious sources in the crowded fields of the Galactic plane. There were 557 stars (481 from the FSC and 76 from the PSC) that passed the initial cross-correlation. Unfortunately, the FSC is only ~80% complete. We therefore cross-correlated all main-sequence *Hipparcos* stars outside the Galactic plane with the PSC using a search radius of 45″. We found an additional 65 stars in the PSC that had 60 μm detections but were unidentified in the FSC. Most of these stars from the PSC were detected at 12 μm (but not 60 μm) in the FSC. In contrast, Silverstone (2000) cross-correlated *Hipparcos* and *IRAS* FSC sources only. Our correlation with the *IRAS* FSC and PSC left a collection of 622 main-sequence stars identified in the *Hipparcos* catalog that had 60 μm counterparts detected by *IRAS*.

In young and massive main-sequence stars, significant IR flux arises from free-free emission. Such stars, namely spectral types O1–B5, were excluded from our sample by rejection of objects with $B - V < -0.15$. Then a distance cut of 120 pc was applied to our sample to avoid contaminations arising from star-forming regions and interstellar cirrus as described, for example, in Kalas et al. (2002) (see below).

A visual inspection of the remaining excess candidates for the presence of a background galaxy was conducted by correlating the FSC and PSC catalogs with NASA's Extragalactic Database (NED) in Digital Sky Survey (DSS) images. Any star with a noticeable galaxy within the 3 σ *IRAS* positional error ellipse was removed from our sample, and any star with a bright star within the 3 σ error ellipse was flagged for further checking of its SED. Since NED is not complete, we also carefully checked any DSS optical extended sources (mainly galaxies) that were not included in NED. Using the long format of the FSC catalog, Silverstone (2000) compared the 60 μm position to the stellar position and excluded stars whose 60 μm offsets are >30″. Instead of imposing such a strict constraint on our sample, we exclude stars only if their 60 μm offsets are greater than the 3 σ *IRAS* positional error. For all FSC sources, we carefully checked their 60 μm positions against any galaxy or bright nearby star.

For stars with apparent detections in the *IRAS* 100 μm band, we tested for possible contamination from interstellar cirrus. Some relatively distant, previously known, IR-excess candidates are contaminated by interstellar cirrus (Kalas et al. 2002). We checked the *IRAS* cirrus flag of all 100 μm sources and rejected those with cirrus flag > 3 except HIP 77542. HIP 77542 had significant excess at all wavelengths and was fit nicely with a single blackbody temperature (Paper I).

A fully automated SED fitting technique using a theoretical atmospheric model (Hauschildt et al. 1999) was used to predict stellar photospheric fluxes. This fit technique is unlike previous excess searches that use the "empirical" color of main-sequence stars to estimate stellar photospheric fluxes. For each star, fluxes at B, V, J, H, and K_s were employed to fit the model spectra of a stellar photosphere. The standard B and V magnitudes were obtained by converting Tycho B and V magnitudes using Table 2 in Bessell (2000). For the 10 *Hipparcos* objects that did not have observed Tycho B and V magnitudes, B and V values were obtained from SIMBAD. Observed J, H, and K_s magnitudes came from the Two Micron All Sky Survey (2MASS) catalog. When any star was brighter than 5th magnitude at J, H, or K_s in 2MASS, we set its uncertainty to 0.400 mag. The zero magnitudes in Cox (2000) were used to convert the observed magnitudes into a flux density (janskys). The current Hauschildt et al. stellar photosphere model (T. Barman 2006, private communication) is available for effective temperatures from 1700 to 10,000 K (in 100 K increments from 1700 to 3000 K and in 200 K increments from 3000 to 10,000 K). The stellar radius and effective temperature were used as free parameters to fit the observed fluxes with a χ^2 minimization method.

We created model fluxes at each band by convolving each filter function with the model spectra. This method provides a more accurate representation of the observed flux especially where the passband includes significant spectral features such as the Balmer jump. Comparing the best-fit model spectra with the observed fluxes, we found that the model spectra always overestimated the *B*- and *V*-band fluxes. This perhaps arises from some missing opacity sources in the *B* and *V* bands of the model spectra. For consistency, we manually set the uncertainties of *B*- and *V*-band magnitude to 0.25 if the given uncertainty value is smaller than 0.25 mag to ensure a better fit.

Once the stellar photosphere was modeled, a dust component was fit with a blackbody curve. *IRAS* upper limits were not included in the dust fitting, but we mandated that the upper limits are always above the estimated total (star and dust) flux. Temperature-dependent *IRAS* color corrections should be carefully considered. Both the stellar photosphere and dust emission contribute to the observed *IRAS* flux as follows:

$$F_{IRAS}^{\rm obs} = F_{\rm phot}^{\rm unc} + F_{\rm dust}^{\rm unc}, \tag{1}$$

where the subscript "unc" stands for "uncorrected." Thus, accurate estimation of a color correction value requires not only the flux of the stellar photosphere but also that of the dust, which is obtained through the blackbody fitting. But the problem is that both dust flux and the color correction are a function of dust temperature, which requires an iterative process to determine the dust temperature in color-corrected *IRAS* dust flux. Instead we obtained the dust temperature by fitting the uncorrected *IRAS* fluxes. First, we "colored" the stellar photosphere (eq. [2]) by multiplying the appropriate color correction terms ($K_{\rm star}$) before subtracting the stellar photosphere (eq. [3]):

$$F_{\rm phot}^{\rm unc} = F_{{\rm phot},m} K_{\rm star}, \tag{2}$$

$$F_{{\rm dust},m}^{\rm unc} = F_{IRAS}^{\rm obs} - F_{{\rm phot},m} K_{\rm star}, \tag{3}$$

where the subscript *m* stands for "model." Then we fit the remaining *IRAS* fluxes with the colored blackbody curve (eq. [4]),

$$F_{{\rm dust},m}^{\rm unc} = F_{{\rm dust},m} K_{\rm dust}. \tag{4}$$

By combining equations (3) and (4) and using the stellar photosphere model described above, we obtained the best-fit temperatures of the stellar and dust emission. Then the correct total *IRAS* color correction terms were calculated by estimating the fractional color terms using a weighted average of photosphere and dust fluxes at each wavelength (eq. [5]):

$$K_{\rm tot} = C_1 K_{\rm star}^{\rm bf} + C_2 K_{\rm dust}^{\rm bf}, \tag{5}$$

where C_1 and C_2 are the fractional contributions of the stellar photosphere and dust to the total measured flux,

$$F_{IRAS}^{\rm true} = F_{IRAS}^{\rm obs} / K_{\rm tot}. \tag{6}$$

In displaying the *IRAS* observed magnitudes, we applied the prorated color correction terms to the *IRAS* measurements (eq. [6]). As in photosphere fitting, we created synthetic fluxes at each *IRAS* band by convolving *IRAS* filter functions with the blackbody curve.

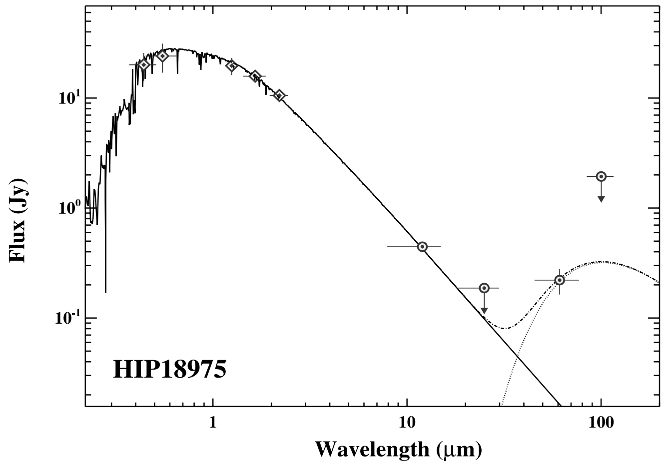

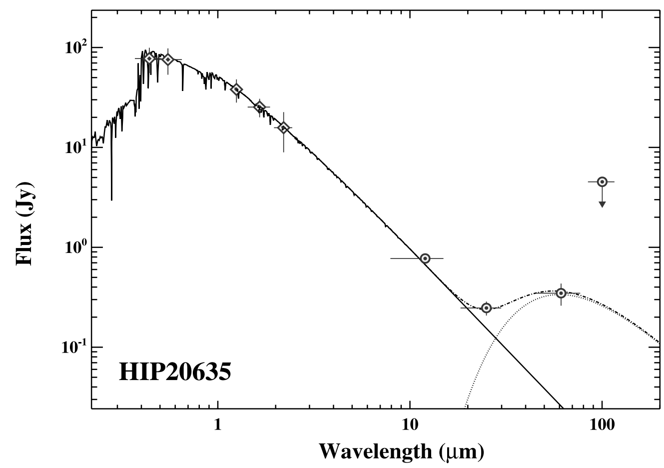

Figs. 2.28 and 2.31 SEDs for HIP 18975 and 20635.

Fig. Set 2.—SED of Hyades stars. Fitting parameters (e.g., $R_\star$, $T_\star$, $R_{\rm dust}$, $T_{\rm dust}$) of each star are given in Table 2, which also gives cautionary notes so that the apparent 60 μm excesses seen in these SEDs cannot be regarded as definite until confirmed with additional data. SEDs of the remaining IR-excess stars are available in the electronic edition. [*See the electronic edition of the Journal for color panels 2.1–2.146 of this figure.*]

SED fits were performed for all identified *IRAS* and *Hipparcos* stars, yielding very precise estimation of stellar photospheric fluxes (Fig. Set 2). When available, additional fluxes from *ISO*[3] and/or *Spitzer*[4] measurements were used to better fit dust components. Four objects were dropped from our list due to possible cirrus contamination or no 60 μm excess based on *ISO* measurements reported in Silverstone (2000). For some objects, *Spitzer* Multiband Imaging Photometer (MIPS) data are available in the public archive but were not published. In such cases, we extracted photometry from MIPS pipeline data at 24 and 70 μm. No photometry was attempted on MIPS 160 μm pipeline data because of heavy contamination from a known "blue leak."

Several Class I and II pre–main-sequence (PMS) stars were found from our SED fits, in which a typical SED of a Class I/II

[3] *ISO* measurements were taken from Silverstone (2000) and Habing et al. (2001).

[4] *Spitzer* MIPS measurements were taken from the references given in § 3.

TABLE 1

Hipparcos Class I and II Pre–Main-Sequence Stars within 120 pc

HIP	HD	Other	Sp. Type	V (mag)	Distance (pc)
17890..............	275877	XY Per	A2 IIev	9.44	120.0
23873..............	240764	RW Aur A	G5 V:e. . .	10.3	70.5
26295..............	36910	CQ Tau	F2 IVe	10.7	99.5
56354..............	100453	. . .	A9 Ve	7.79	111.5
56379..............	100546	KR Mus	B9 Vne	6.70	103.4
58520..............	104237	DX Cha	A:pe	6.60	116.1
82323..............	. . .	V1121 Oph	K5	11.25	95.1

PMS star shows large B and V fluxes above the model spectrum and strong, but flat, excess in the IR. Because we are searching for IR excess among main-sequence stars, Class I and II PMS stars were subsequently eliminated from our sample. For completeness, the *IRAS*-identified *Hipparcos* Class I and II PMS stars within 120 pc are listed in Table 1.

Many sources that passed the visual check, especially nearby stars, showed no IR excess in their SED. Color-corrected *IRAS* fluxes were compared to the estimated photospheric fluxes. Stars with no IR excess $[(F_{IRAS} - F_{\rm phot})/\sigma_{IRAS} < 2.5]$ were eliminated except HIP 71284, where σ_{IRAS} is the *IRAS* 60 μm flux density uncertainty. IR excess in HIP 71284 was confirmed by an *ISO* observation (Paper I). One hundred forty-six stars had IR excess $[(F_{IRAS} - F_{\rm phot})/\sigma_{IRAS} > 3.0]$, and nine stars showed marginal IR excess $[2.5 < (F_{IRAS} - F_{\rm phot})/\sigma_{IRAS} < 3.0]$. These marginal IR excess stars fall into a statistical domain in which ~0.5% of non-excess stars may produce a false excess, assuming Gaussian noise under *pure statistical detection errors*. Recent *Spitzer* observations show that three stars (HIP 65109, HIP 105090, and HIP 105858) that had marginal IR excess from *IRAS* are not IR-excess stars. In addition, even some stars with $(F_{IRAS} - F_{\rm phot})/\sigma_{IRAS} > 3.0$ turn out to be false positives. For example, HIP 83137, passing all the tests above, had $(F_{IRAS} - F_{\rm phot})/\sigma_{IRAS} = 4.3$ and was considered one of the better new IR-excess candidates. However, recent *Spitzer* MIPS observations found no excess emission at 70 μm at HIP 83137, along with six other similar stars (HIP 8102, HIP 42913, HIP 49641, HIP 75118, HIP 98025, and HIP 104206).

All six bogus excess stars had *IRAS* excess emission detected at 60 μm only. To date, *Spitzer* has looked at a total of 26 such stars in our sample, producing a false excess rate of 27% (7/26). Applying this rate to the remaining 54 stars with IR excess emission detected at *IRAS* 60 μm alone, we anticipate that about 15 objects, or 10% (15/146)[5] of our sample, may turn out as non-excess stars.

Generally, a bogus excess can be produced in two quite different ways. One way is that a real, background, far-IR source is present in the beam when *IRAS* pointed toward a *Hipparcos* star. The other is that a 3 σ noise bump happens to fall near a *Hipparcos* star. Apparent excess sources rejected for both reasons are listed in Table 4. The number of real background sources (mostly galaxies) anticipated in our sample can be estimated in a way analogous to that described in § 2 of Zuckerman et al. (1995b); such an estimate agrees reasonably with the number of background galaxies listed in Table 4.

If the background noise has a normal distribution, then we anticipate that about 1 star in 500 could be contaminated by a 3.1 σ noise fluctuation. After our distance and color cuts described above, we were left with ~25,800 *Hipparcos* dwarfs. Thus, of these, ~50 might be contaminated by a noise fluctuation. Some constraint is supplied by examination of *IRAS* Scan Processing and Integration (SCANPI) traces that sometimes show the 60 μm peak position to be displaced from the stellar position. Background noise could be responsible, in total, for ~20 *Hipparcos* stars listed in Table 4.

Nearby M-type stars are now known not to be strong IR-excess sources (e.g., Plavchan et al. 2005; Riaz et al. 2006); indeed the only one listed in Table 2 is AU Mic, which is a very young star. There are ~900 M-type dwarf stars in the *Hipparcos* catalog, and the only one other than AU Mic that appeared in our cross-correlation with *IRAS* was AX Mic, in which, however, a *Spitzer* MIPS observation showed that there is no 70 μm excess. According to the above estimates, we might have expected two bogus *IRAS* associations in these 900 stars, in reasonable agreement with the one, AX Mic, that was actually found.

We finally present 146 *IRAS*-identified *Hipparcos* IR-excess dwarfs in this paper. Among them 33 stars are newly identified as IR-excess stars from our survey, and only 2 objects out of these 33 newly identified IR-excess stars have marginal IR-excess $[2.5 < (F_{IRAS} - F_{\rm phot})/\sigma_{IRAS} < 3.0]$.

3. OVERVIEW OF PREVIOUS *IRAS*, *ISO*, AND *SPITZER* SURVEYS FOR DUSTY DEBRIS DISKS

Comparison of *IRAS* with *ISO* and *Spitzer* demonstrates the power of all-sky surveys. Notwithstanding that *IRAS* flew more than 20 years ago, through careful analysis of its database, we have been able to discover as many as 33 main-sequence *Hipparcos* stars with previously unrecognized dusty debris disks detected at 60 μm wavelength. In comparison, only 22 new 60 μm excess stars were discovered in all *ISO* programs, while ~20 new 70 μm excess stars were announced in the 2004 and 2005 *Spitzer*-based literature (see below for references). Although *ISO* and *Spitzer* have higher sensitivities than *IRAS*, they are both pointed satellites with a much smaller sky coverage.

IRAS surveys and, significantly, some of their limitations are summarized in § 1 of the present paper and in § 3 of Zuckerman (2001). Previous to the present study, Silverstone (2000) represented the most comprehensive search of the *IRAS* catalogs for Vega-like 60 μm excess stars. However, Silverstone's primary goal was to use *ISO* to detect dust at F- and G-type stars inconclusively detected by *IRAS* at 60 μm. He did not analyze his *IRAS* findings, and his search never reached publication. Thus, no *IRAS* survey published prior to 2005 is germane to issues addressed in the present paper.

ISO was a pointed satellite of modest sensitivity, and surveys by various groups added relatively few new Vega-like stars. Decin et al. (2003) give a comprehensive account of these surveys, a major goal of which was characterization of the time dependence of the Vega phenomenon. One limitation of these studies, as noted by Decin et al., is the quite uncertain ages of many of the excess stars. Indeed, we disagree with some of the ages in Table 1 of Decin et al. They describe some limitations to the results presented by Spangler et al. (2001), limitations due, in part, to the poorer than expected sensitivity of *ISO*.

A next advance was by Manoj & Bhatt (2005), who focused on deducing the lifetimes and temporal evolution of the dust around the Vega-like stars. In an original analysis, they considered the relative sky-plane velocity dispersions of the Vega-like stars and of *Hipparcos* stars in general to demonstrate that, at any given spectral type, the Vega-like stars are, on average, younger than the general population of field stars. They also

[5] 146 = 146 + 9 (with marginal IR excess) + HIP 71284 − 10 bogus stars.

TABLE 2

Stars with Dusty Debris Disks

HIP (1)	HD (2)	Sp. Type (3)	V (mag) (4)	D (pc) (5)	$R_\star$ ($R_\odot$) (6)	$T_\star$ (K) (7)	$T_{\rm dust}$ (K) (8)	$R_{\rm dust}$ (AU) (9)	Angle (arcsec) (10)	τ (11)	Dust Mass $M_\oplus$ (12)	Age (Myr) (13)	Age Method[a] (14)	Dust Excess Confirmation (15)	Notes[b] (16)
746	432	F2 III–IV	2.3	16.7	3.36	7200	120	28	1.68	2.50E−05	2.15E−03	1000	a, b, c	. . .	
1185	1051	A7 III	6.8	88.3	1.87	8000	40	173	1.97	4.32E−04		600	a, d	. . .	
4267	5267	A1 Vn	5.8	112.6	2.67	10000	85	86	0.76	8.77E−05		200	a, d	. . .	1, 2, 3
5626	6798	A3 V	5.6	83.5	2.25	10000	75	93	1.12	1.49E−04	1.41E−01	200?	a, d	. . .	
6686	8538	A5 Vv	2.7	30.5	3.90	8400	85	88	2.90	5.95E−06		600	a, d	. . .	
6878	8907	F8	6.7	34.2	1.19	6600	45	59	1.74	2.08E−04	3.84E−02[c]	200?	a, b, c	MIPS, *ISO*	
7345	9672	A1 V	5.6	61.3	1.66	10000	80	60	0.99	7.94E−04	3.13E−01	20?	Z95b	. . .	4
7805	10472	F2 IV/V	7.6	66.6	1.28	7000	70	30	0.45	3.68E−04	3.39E−02	30	Z01b	MIPS	
7978	10647	F8 V	5.5	17.4	0.99	6400	65	22	1.28	4.16E−04	2.21E−02	300?	a, b, c	. . .	
8122	10638	A3	6.7	71.7	1.57	8200	85	33	0.47	4.69E−04		100	a, d	. . .	
8241	10939	A1 V	5.0	57.0	1.94	10000	75	80	1.41	6.44E−05	4.52E−02	200?	a, d	MIPS	2, 5
9570	12471	A2 V	5.5	113.5	3.28	10000	85	105	0.93	1.01E−04		600	a, d	. . .	
10054	12467	A1 V	6.0	68.4	1.73	9200	60	94	1.38	8.72E−05	8.45E−02	200??	a, d	MIPS	2
10670	14055	A1 Vnn	4.0	36.1	1.96	10000	75	80	2.24	7.18E−05	2.86E−02[c]	100?	a, d	. . .	
11360	15115	F2	6.8	44.8	1.23	7200	65	35	0.78	5.08E−04	4.48E−02[c]	100?	a, b, c	MIPS, *ISO*	
11486	15257	F0 III	5.3	47.6	2.26	7400	85	39	0.84	1.14E−04	1.90E−02	≲1000	a, d	. . .	2
11847	15745	F0	7.5	63.7	1.21	7600	85	22	0.35	1.72E−03	9.13E−02	30?	d	MIPS, *ISO*	
12361	16743	F1 III/IV	6.8	60.0	1.58	7200	40	119	1.98	5.94E−04		200	a, d	MIPS	
12964	17390	F3 IV/V	6.5	45.1	1.39	7200	55	55	1.23	2.00E−04	8.52E−02	300??	a	MIPS	
13005	. . .	K0	8.1	67.7	2.17	5200	85	18	0.28	1.11E−03		. . .	b	. . .	6, 7
13141	17848	A2 V	5.3	50.7	1.88	8200	55	97	1.92	6.39E−05	6.59E−02	100	a, d	MIPS	
14576	19356	B8 V	2.1	28.5	4.13	9200	250	13	0.46	1.67E−05		. . .	. . .	MIPS	2, 7, 8
15197	20320	A5m	4.8	36.8	2.00	7800	95	31	0.85	2.046E−05	2.59E−03	400?	a, d	MIPS	9
16449	21997	A3 IV/V	6.4	73.8	1.57	9000	60	82	1.12	4.9E−04	2.24E−01[c]	50?	a, d	MIPS	
16537	22049	K2 V	3.7	3.2	0.69	5200	40	27	8.47	8.30E−05	2.61E−03[c]	730	S00	MIPS, *ISO*	
18437	24966	A0 V	6.9	103.5	1.50	10000	85	48	0.47	2.58E−04		10	d	. . .	
18859	25457	F5 V	5.4	19.2	1.19	6400	85	16	0.81	1.31E−04	3.68E−03	30	a, b, c	MIPS, *ISO*	
18975	25570	F2 V	5.4	36.0	1.83	7000	85	28	0.80	8.86E−05		600	Hyades	. . .	2, 3
19704	27346	A9 IV	7.0	114.5	2.57	7600	70	70	0.62	2.61E−04		600?	a, d	. . .	2, 10, 11
19893	27290	F4 III	4.3	20.3	1.65	7200	80	31	1.53	2.30E−05		300?	a, b	. . .	12
20635	27934	A7 IV–V	4.2	47.0	2.60	9000	85	67	1.44	4.72E−05		600	Hyades	. . .	2, 10
21604	29365	B8 V	5.8	110.7	3.06	8800	75	97	0.88	3.78E−04		200?	a, d	. . .	2, 8
22226	30447	F3 V	7.9	78.1	1.31	7200	65	37	0.48	8.85E−04	1.33E−01	≲100	a	MIPS	
22439	30743	F3/F5 V	6.3	35.4	1.46	6400	40	86	2.45	2.28E−04		>1000	a, b, c	. . .	2, 13
22845	31295	A0 V	4.6	37.0	1.67	9000	80	49	1.33	8.44E−05	2.22E−02	100?	a, d	MIPS	
23451	32297	A0	8.1	112.1	1.24	8400	85	28	0.25	5.38E−03	4.62E−01	20?	d	. . .	
24528	34324	A3 V	6.8	85.8	1.59	8800	100	28	0.33	1.72E−04	1.48E−02	200?	d	. . .	
25197	34787	A0 Vn	5.2	104.3	3.26	10000	120	52	0.50	6.97E−05	2.07E−02	400?	a, d	. . .	2
25790	36162	A3 Vn	5.9	105.6	2.92	8800	85	72	0.69	2.49E−04		600?	a, d	. . .	14
26453	37484	F3 V	7.2	59.5	1.36	7000	90	19	0.32	2.85E−04	1.13E−02	30	a, b, c	MIPS	
26966	38206	A0 V	5.7	69.2	1.63	10000	85	53	0.76	1.99E−04	6.13E−02	50	a, d	MIPS	
27072	38393	F7 V	3.6	9.0	1.18	6600	90	15	1.64	7.71E−06	4.48E−04[c]	>1000??	a, b	MIPS	
27288	38678	A2 Vann	3.5	21.5	1.65	9000	220	6	0.30	1.34E−04		100	a, d	MIPS	
27321	39060	A3 V	3.9	19.3	1.37	8600	110	19	1.01	2.64E−03	8.99E−02[c]	12	β Pic	MIPS	
27980	39833	G0 III	7.7	46.7	1.23	6000	70	20	0.45	2.79E−03		700	a, b, c	. . .	2, 15
28103	40136	F1 V	3.7	15.0	1.52	7400	185	6	0.38	2.04E−05		300?	a, b, d	MIPS	
28230	40540	A8 IVm	7.5	89.9	1.45	7800	90	25	0.28	6.06E−04		200	d	. . .	2, 16
32480	48682	G0 V	5.2	16.5	1.08	6400	60	29	1.73	8.93E−05		600??	a, b	MIPS	17
32775	50571	F7 III–IV	6.1	33.2	1.38	6600	45	68	2.08	1.63E−04	8.26E−02	300?	a, b, c	MIPS	
33690	53143	K0 IV–V	6.8	18.4	0.88	5400	80	9	0.50	1.97E−04	1.87E−03	300?	a, b, c	MIPS	
34276	54341	A0 V	6.5	92.9	1.59	10000	85	51	0.55	2.01E−04		10	d	. . .	18
34819	55052	F5 IV	5.8	107.1	4.74	6800	45	251	2.35	1.01E−04		300??	a, c	. . .	2, 3
35550	56986	F0 IV. . .	3.5	18.0	2.13	7200	60	71	3.95	8.93E−06	4.94E−03	400??	a, b, d	MIPS	9
36906	60234	G0	7.6	108.6	2.78	6200	85	34	0.32	4.29E−04		600?	a, b	. . .	2
36948	61005	G3/G5 V	8.2	34.5	0.81	5600	60	16	0.48	2.58E−03	7.24E−02	100?	a, b, c	MIPS	
39757	67523	F2mF5 IIp	2.8	19.2	3.41	6800	85	50	2.64	5.38E−06		≳2000	a, b, c	. . .	
40938	70298	F2	7.2	70.9	1.77	6800	85	26	0.37	3.54E−04		>3000	a, b	. . .	2
41152	70313	A3 V	5.5	51.4	1.54	10000	80	56	1.09	5.24E−05	1.80E−02	200	a, d	MIPS	
41307	71155	A0 V	3.9	38.3	2.02	10000	130	29	0.73	4.09E−05	3.77E−03	100	a, d	MIPS	
42028	72660	A1 V	5.8	100.0	2.39	10000	85	77	0.77	7.07E−05		200	a, d	. . .	2
42430	73752	G3/G5 V	5.1	19.9	1.73	5800	80	21	1.06	3.21E−05	1.55E−03	>600	S00	. . .	19
43970	76543	A5 III	5.2	49.0	1.86	8800	85	46	0.94	1.04E−04		400?	a, d	. . .	2
44001	76582	F0 IV	5.7	49.3	1.73	8000	85	35	0.72	2.22E−04		300??	a, d	. . .	

TABLE 2—*Continued*

HIP (1)	HD (2)	Sp. Type (3)	V (mag) (4)	D (pc) (5)	$R_\star$ ($R_\odot$) (6)	$T_\star$ (K) (7)	T_{dust} (K) (8)	R_{dust} (AU) (9)	Angle (arcsec) (10)	τ (11)	Dust Mass $M_\oplus$ (12)	Age (Myr) (13)	Age Method[a] (14)	Dust Excess Confirmation (15)	Notes[b] (16)
45758........	80425	A5	6.6	98.1	2.43	7600	85	45	0.46	2.70E−04		300?	a, d	. . .	2
48164........	84870	A3	7.2	89.5	1.59	8000	85	32	0.37	5.48E−04		100	d	. . .	1
48541........	85672	A0	7.6	93.1	1.19	9200	85	32	0.35	4.82E−04		30?	a, d	. . .	
51438........	91375	A2 III	4.7	79.4	3.10	10000	85	99	1.26	2.42E−05		400??	a, d	. . .	20
51658........	91312	A7 IV	4.7	34.3	1.84	8200	40	179	5.23	1.06E−04		200	a, d	. . .	9
52462........	92945	K1 V	7.7	21.6	0.77	5200	45	23	1.11	6.74E−04	3.91E−02	100	SBZ	MIPS	
53524........	95086	A8 III	7.4	91.6	1.49	8200	85	32	0.35	1.49E−03		50	d	. . .	2, 21
53910........	95418	A1 V	2.3	24.3	2.84	10000	120	45	1.88	1.23E−05	2.73E−03	500	UMa	. . .	
53911........	. . .	K8 Ve	11.1	56.4	1.11	4000	140?	2	0.04	>2.17E−01		8	TW Hya	MIPS	
55505........	98800	K4 V	9.1	46.7	1.97	4200	160	3	0.07	1.12E−01		8	TWA	MIPS	9
56253........	99945	A2m	6.1	59.8	1.72	8200	85	37	0.62	1.04E−04		300?	a, d	. . .	
56675........	101132	F1 III	5.6	42.1	1.95	7000	50	88	2.11	1.42E−04		300	a, b, c, d	. . .	2, 22
57632........	102647	A3 Vvar	2.1	11.1	1.67	8800	160	11	1.06	4.25E−05	5.64E−04	50	S01	MIPS	
60074........	107146	G2 V	7.0	28.5	0.97	6200	55	29	0.97	9.50E−04	8.99E−02[c]	≲100	a, b, c	MIPS	
61174........	109085	F2 V	4.3	18.2	1.62	6800	180	5	0.30	1.20E−04		300	a, b, c	MIPS	
61498........	109573	A0 V	5.8	67.1	1.59	10000	110	30	0.46	4.43E−03	2.11E−01[c]	8	HR 4796A	MIPS	
61782........	110058	A0 V	8.0	99.9	1.09	8800	130	11	0.12	2.54E−03	3.37E−02	10?	LCC	IRS	21
61960........	110411	A0 V	4.9	36.9	1.49	9000	85	38	1.05	6.23E−05	9.86E−03	100??	a, d	MIPS	
63584........	113337	F6 V	6.0	37.4	1.50	7200	100	18	0.48	1.01E−04	3.59E−03	50?	a, b	. . .	23
64375........	114576	A5 V	6.5	112.6	2.63	8200	85	56	0.51	3.90E−04		600	a, d	. . .	1
64921........	115116	A7 V	7.1	85.4	1.53	8400	80	39	0.46	3.39E−04		100?	a, d	. . .	
68101........	121384	G8 V	6.0	38.1	2.95	5200	45	91	2.41	2.47E−04		>3000	a, b, c	. . .	
68593........	122652	F8	7.2	37.2	1.07	6400	60	28	0.76	1.36E−04	1.17E−02	300?	a, b, c	MIPS	
69682........	124718	G5 V	8.9	61.3	0.98	5800	85	10	0.17	2.11E−03		>500	a, b, c	. . .	24
69732........	125162	A0sh	4.2	29.8	1.72	9000	100	32	1.09	5.22E−05	5.86E−03	200?	a, d	MIPS	
70090........	125473	A0 IV	4.1	75.8	3.98	10000	120	64	0.85	2.11E−05	9.48E−03	300	a, d	. . .	
70344........	126265	G2 III	7.2	70.1	2.12	6200	85	26	0.37	3.85E−04		>500	a, b	. . .	
70952........	127821	F4 IV	6.1	31.7	1.30	6800	50	55	1.76	2.58E−04	8.26E−02[c]	200?	a, b	. . .	
71075........	127762	A7 IIIvar	3.0	26.1	3.08	8000	55	151	5.80	1.04E−05		1000	a, d	. . .	
71284........	128167	F3 Vwvar	4.5	15.5	1.39	6600	40	88	5.70	4.91E−06	6.37E−03[c]	1000??	a, b, c	MIPS, *ISO*	
73049........	131625	A0 V	5.3	75.8	2.49	9000	85	64	0.86	7.39E−05		200	a, d	. . .	2
73145........	131835	A2 IV	7.9	111.1	1.26	8600	90	26	0.24	3.07E−03	2.28E−01	10	d	. . .	25
73473........	132742	B9.5 V	4.9	93.3	3.94	8800	150	31	0.34	7.22E−05	7.61E−03	500	a, d	. . .	2, 8, 26
73512........	132950	K2	9.1	30.4	0.75	4800	85	5	0.18	1.17E−03		3000??	. . .	. . .	2
74596........	135502	A2 V	5.3	69.4	2.24	10000	65	123	1.77	3.26E−05		200	a, d	. . .	
74946........	135382	A1 V	2.9	56.0	5.86	9400	50	481	8.60	9.29E−06		700??	a, d	. . .	
76127........	138749	B6 Vnn	4.2	95.3	4.16	10000	75	171	1.80	1.99E−05		200?	a, d	. . .	
76267........	139006	A0 V	2.2	22.9	2.72	10000	190	17	0.76	2.41E−05	7.64E−04	500	a, b, d	MIPS	8
76375........	139323	K3 V	7.6	22.3	0.85	5200	29	64	2,87	7.86E−04		5000??	a, b	. . .	2, 27
76635........	139590	G0 V	7.5	55.1	1.40	6200	85	17	0.31	3.93E−04		5000??	a, b	. . .	
76736........	138965	A5 V	6.4	77.3	1.47	9600	140	16	0.21	1.17E−04	3.28E−03	20	a, d	MIPS	2
76829........	139664	F5 IV–V	4.6	17.5	1.26	7000	75	25	1.46	1.15E−04	7.88E−03	200?	a, b, c	MIPS	
77163........	140775	A1 V	5.6	117.8	3.25	10000	40	472	4.01	1.39E−04		600	a, d	. . .	28
77542........	141569	B9	7.1	99.0	1.49	9200	110	24	0.25	1.12E−02	3.32E−01[c]	5	HD 141569	MIPS	
78554........	143894	A3 V	4.8	54.3	2.27	9000	45	211	3.89	4.64E−05		300	a, d	. . .	
81126........	149630	B9 Vvar	4.2	92.7	4.91	9400	80	157	1.70	3.01E−05		700	a, d	. . .	1
81641........	150378	A1 V	5.8	92.9	2.23	10000	95	57	0.62	1.24E−04	4.42E−02	200	a, d	. . .	1
81800........	151044	F8 V	6.5	29.4	1.21	6200	55	35	1.22	8.30E−05	1.11E−02	>500	a, b	MIPS, *ISO*	
82405........	151900	F1 III–IV	6.3	59.8	2.30	6600	85	32	0.54	2.98E−04		>1000	a, d	. . .	2, 10
83480........	154145	A2	6.7	94.9	1.99	8400	85	45	0.48	4.28E−04		300?	d	. . .	28
85157........	157728	F0 IV	5.7	42.8	1.43	8600	90	30	0.71	2.67E−04	2.63E−02	100?	a, d	. . .	
85537........	158352	A8 V	5.4	63.1	2.52	8400	70	85	1.35	6.81E−05	5.39E−02	600?	a, d	MIPS	
87108........	161868	A0 V	3.7	29.1	1.91	9400	85	54	1.87	7.84E−05	2.51E−02	200?	a, d	MIPS	
87558........	162917	F4 IV–V	5.8	31.4	1.50	6600	85	20	0.67	2.49E−04		400?	a, b, c	. . .	
88399........	164249	F5 V	7.0	46.9	1.27	6800	70	27	0.60	1.03E−03	8.23E−02	12	Z01a	MIPS, *ISO*	
90185........	169022	B9.5 III	1.8	44.3	6.66	10000	100	155	3.50	4.46E−06		300??	a, b, d	. . .	
90936........	170773	F5 V	6.2	36.1	1.34	7000	50	61	1.69	4.63E−04	1.89E−01	200?	a, b, c	MIPS, *ISO*	
91262........	172167	A0 Vvar	0.0	7.8	2.58	10000	80	93	12.10	2.14E−05	8.37E−03[c]	220	Vega	MIPS	
92024........	172555	A7 V	4.8	29.2	1.52	8000	320	2	0.08	8.10E−04		12	Z01a	MIPS	
93542........	176638	A0 Vn	4.7	56.3	2.11	10000	120	34	0.60	9.70E−05	1.23E−02	200?	a, d	. . .	
95261........	181296	A0 Vn	5.0	47.7	1.61	9600	150	15	0.32	2.13E−04	5.25E−03	12	Z01a	MIPS, *ISO*	
95270........	181327	F5/F6 V	7.0	50.6	1.39	6600	75	25	0.50	3.47E−03	2.38E−01	12	Z01a	MIPS	
95619........	182681	B8/B9 V	5.7	69.1	1.71	10000	85	55	0.80	1.95E−04		50?	a, d	. . .	
96468........	184930	B5 III	4.3	94.3	4.01	10000	60	259	2.75	3.52E−05		. . .	. . .	. . .	2, 7

TABLE 2—*Continued*

HIP (1)	HD (2)	Sp. Type (3)	V (mag) (4)	D (pc) (5)	$R_\star$ ($R_\odot$) (6)	$T_\star$ (K) (7)	T_{dust} (K) (8)	R_{dust} (AU) (9)	Angle (arcsec) (10)	τ (11)	Dust Mass $M_\oplus$ (12)	Age (Myr) (13)	Age Method[a] (14)	Dust Excess Confirmation (15)	Notes[b] (16)
99273..........	191089	F5 V	7.2	53.5	1.39	6600	95	15	0.29	1.39E−03	3.43E−02	$\lesssim$30	a, b, c	MIPS	9
99473..........	191692	B9.5 III	3.2	88.0	6.63	10000	85	213	2.43	6.60E−06		500?	a, d	. . .	
101612........	195627	F1 III	4.8	27.6	1.70	7400	65	51	1.86	1.11E−04	3.17E−02	200?	a, d	MIPS	
101769........	196524	F5 IV	3.6	29.9	3.63	6800	130	23	0.77	1.56E−05	9.05E−04	200??	a, b, c	. . .	2, 9
101800........	196544	A2 V	5.4	54.3	1.65	9000	100	31	0.57	3.86E−05	4.07E−03	30	a, d	MIPS	9
102409........	197481	M1 Ve	8.8	9.9	0.86	3500	50	9	0.98	3.64E−04	8.80E−03[c]	12	Z01a	MIPS	
103752........	199475	A2 V	6.4	83.3	1.83	8800	85	45	0.55	2.45E−04		200	a, d	. . .	2
105570........	203562	A3 V	5.2	110.4	4.02	9000	85	104	0.95	8.80E−05		600?	a, d	. . .	1
106741........	205674	F3/F5 IV	7.2	52.6	1.22	7200	85	20	0.39	3.96E−04		300?	a, b	. . .	
107022........	205536	G8 V	7.1	22.1	0.89	5600	80	10	0.46	2.92E−04	3.20E−03	>500	a, b	. . .	
107412........	206893	F5 V	6.7	38.9	1.24	6600	55	41	1.07	2.72E−04	3.18E−02[c]	200?	a, b	MIPS, *ISO*	
107649........	207129	G2 V	5.6	15.6	0.98	6000	55	27	1.74	1.21E−04	9.67E−03	600	S03	MIPS, *ISO*	
108809........	209253	F6/F7 V	6.6	30.1	1.10	6200	75	18	0.58	7.33E−05	2.60E−03	200??	a, b, c	MIPS, *ISO*	
109857........	211336	F0 IV	4.2	25.7	1.86	7800	65	62	2.41	1.56E−04	6.58E−02	600?	a, c, d	. . .	
110867........	210681	K0 III	8.1	61.8	1.87	5200	85	16	0.26	7.15E−04		. . .	. . .	. . .	2, 7
111278........	213617	F1 V	6.4	52.9	1.57	7600	55	69	1.32	9.35E−05	4.9E−02	600?	a, d	MIPS	
113368........	216956	A3 V	1.2	7.7	1.81	8600	65	73	9.60	7.98E−05	2.41E−02[c]	220	Fomalhaut	MIPS	
114189........	218396	A5 V	6.0	39.9	1.37	7800	50	77	1.94	2.29E−04	1.00E−01[c]	30	a, d	*ISO*	
116431........	221853	F0	7.3	71.2	1.48	7400	85	26	0.37	7.38E−04	5.47E−02	$\lesssim$100	a	MIPS, *ISO*	

NOTES.—Calculations use 1 AU = 215 $R_\odot$. Table 2 is also available in machine-readable form in the electronic edition of the *Astrophysical Journal*.

[a] Age methods: S00: Song et al. (2000); S01: Song (2001); SBZ: Song et al. (2002a); Z95b: Zuckerman et al. (1995a); Z01a: Zuckerman et al. (2001a); Z01b: Zuckerman et al. (2001b); ZW00: Zuckerman & Webb (2000); S03: Song et al. (2003); a: *UVW* (Zuckerman & Song 2004b); b: X-ray emission, e.g., Song et al. (2003); c: lithium age (Song et al. 2003); d: location on an A-star Hertzsprung-Russell diagram (Lowrance et al. 2000).

[b] 1. Binary.

2. New debris disk candidate.
3. Caution: *IRAS* SCANPI shows high background fluctuation near *IRAS* 60 μm detection.
4. HIP 7345 (=49 Cet) is the only known main-sequence A-type star with CO emission detected with a radio telescope (Zuckerman et al. 1995a), thus suggesting a very young age. But its Galactic space motion $UVW = (-23, -17, -4)$ with respect to the Sun is not indicative of extreme youth (U is positive toward the Galactic center).
5. HIP 8241 shows the age of the Pleiades on an A star H-R diagram (Lowrance et al. 2000), but that of the Hyades in *UVW* measurements.
6. There is a galaxy at ~48″ east of HIP 13005 in the cross-scan direction as described in Paper I. However, a more careful check of the *IRAS* 60 μm offset using the FSC long format indicates that both *IRAS* 12 and 60 μm detections have the same offsets away from the galaxy in the same cross-scan direction. Thus, we include HIP 13005 with a caution.
7. No age estimate is given for HIP 13005, HIP 14576, HIP 96468, and HIP 110867.
8. Eclipsing binary of the Algol type.
9. Spectroscopic binary.
10. Caution: *IRAS* SCANPI shows 30″ offset *IRAS* μm detection from the stellar position in in-scan direction.
11. There are two FSC detections for HIP 19704 separated by 34″ in the in-scan direction. One has 12 and 25 μm detections; the other has a 60 μm detection. The long format of FSC locates the 60 μm source on HIP 19704.
12. In addition to the pointlike 60 μm source reported in the FSC, there is an extended optical source 70″ from the *IRAS* position of HIP 19893 in the in-scan direction. Jura et al. (2004) found no strong excess up to 35 μm in this star. Thus, the *IRAS* excess at 60 μm should be regarded with caution.
13. Caution: there is a galaxy 90″ east of HIP 22439.
14. Caution: there is a galaxy 55″ east of the FSC position at the 3 σ edge of the error ellipse, mostly in the cross-scan direction.
15. Caution: *IRAS* FSC detection is 40″ west of HIP 27980, and *IRAS* SCANPI profile is very broad.
16. Caution: there is a galaxy 58″ away from the *IRAS* position of HIP 28230 in the cross-scan direction.
17. There is a *ROSAT* All-Sky Survey X-ray source ~44″ from HIP 32480, but *UVW* indicates an old age.
18. Location on A-star H-R diagram near HR 4796 is suggestive of a 10 Myr age, but the V component of *UVW* (−16, −44, −9; Moór et al. 2006) is quite unlike that of most very young stars.
19. HIP 42430 is a 1.0″ binary.
20. Caution: SCANPI shows a bad profile fit to the 60 μm source.
21. Kouwenhoven et al. (2005) say HIP 53524 and HIP 61782 are Lower Centaurus–Crux members.
22. Caution: *IRAS* SCANPI shows no source detection.
23. The M star companion LDS 2662 to HIP 63584 is very young based on its location on an M_K vs. $V-K$ color-magnitude diagram (e.g., Fig. 2 in Song et al. 2003).
24. Moór et al. (2006) rejected HIP 69682 based on a nearby 2MASS source with an excess in the K_s band. However, no NED-identified extended source exists within 2′ from this star, and the FSC long format indicates that the 60 μm detection falls on the star itself. The Galactic space motion (*UVW*) and absence of lithium and of X-ray emission all point to an old star. There is no evidence on the Digital Sky Survey and 2MASS All Sky QuickLook Images (JHK_s) of a nearby galaxy. Yet τ is very large.
25. HIP 73145 is an Upper Centaurus–Lupus member.
26. HIP 73473 has significant X-ray flux.
27. Caution: there exists a large galaxy at ~80″ east of HIP 76375.
28. Moór et al. (2006) rejected HIP 77163 and HIP 83480 based on their location near the wall of the Local Bubble.

[c] Dust mass measurements are directly from submillimeter observations.

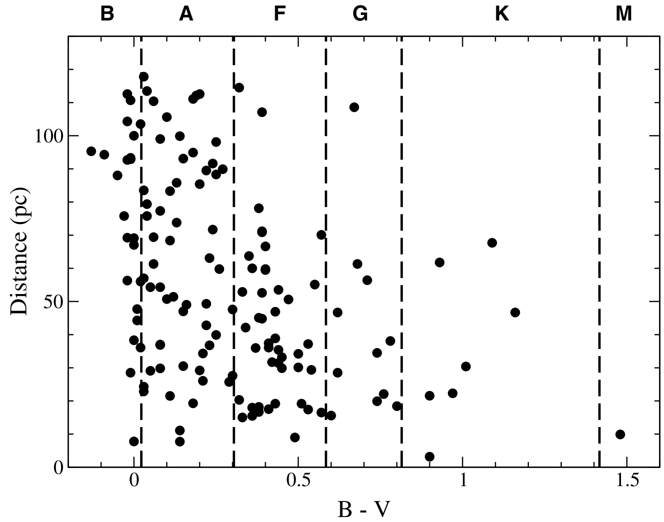

FIG. 3.—Distribution of our 146 candidate excess stars in distance from Earth as a function of $B - V$. As reported before, early-type stars dominate the *IRAS* debris disk systems.

showed that the average τ of the Vega-like stars declines with increasing velocity dispersion, that is, with increasing age. Because their analysis technique is very different from ours and because their sample of excess stars is not called out explicitly in their paper, it is not possible to make a direct comparison between their results and ours. However, wherever their conclusions and ours do overlap, they appear to be consistent.

Most recently, Moór et al. (2006) compiled a list of 60 debris disks with high fractional dust luminosity, $\tau > 10^{-4}$, and within 120 pc of Earth by searching the *IRAS* and *ISO* databases. Forty-eight objects in Moór et al. are included in our survey, while 12 objects are absent. Among those 12 objects missing, four are not *Hipparcos* stars, and six of eight *Hipparcos* stars did not have a detection at 60 μm with *IRAS* and, therefore, did not satisfy our search criteria (§ 2). The remaining two, HD 121812 (HIP 68160) and HD 122106 (HIP 68380), are rejected in the present paper due to possible cirrus contamination and the presence of a nearby galaxy, respectively (see Table 4 for the list of rejected sources). We included five objects (HIP 13005, HIP 25790, HIP 69682, HIP 77163, and HIP 83480) from the Moór et al. list of rejected suspicious objects; our reasoning is discussed in the notes for these individual objects in Table 2.

Five papers that appeared in 2004 or 2005 report *Spitzer* detections at 70 μm for a total of ~20 Vega-like stars that had not previously been detected at 60 μm by *IRAS* and/or *ISO* (Meyer et al. 2004; Chen et al. 2005; Beichman et al. 2005; Low et al. 2005; Kim et al. 2005). Although it is not possible to tell exactly how many stars *Spitzer* pointed toward (searched) at 70 μm in these studies, it appears to be of order a few hundred. Thus, only about 10% of stars reveal far-IR dust emission at levels between *IRAS* and *Spitzer* sensitivities.

4. SAMPLE CHARACTERISTICS

Our IR-excess sample consists of 146 *Hipparcos* dwarfs within 120 pc of Earth. Figure 3 illustrates the distance and $B - V$ distribution of the sample. The relative paucity of debris disks from late-type stars has been previously well established and attributed to the *IRAS* detection threshold (Song et al. 2002b). However, grain removal by stellar wind drag at M-type stars could also be implicated (Plavchan et al. 2005).

Our stars are listed in Table 2, including 51 out of 58 stars from Paper I. The remaining seven objects had *ISO* detections but lacked an *IRAS* 60 μm detection, an absolute requirement in the present paper. The *Hipparcos* and the HD numbers are listed in columns (1) and (2), respectively. Spectral type, V magnitude, and distance from Earth from the *Hipparcos* main catalog are given in columns (3), (4), and (5), respectively. The stellar radius and temperature, $R_\star$ (col. [6]) and $T_\star$ (col. [7]), are obtained from the SED fit. As described in § 2, the fitting process was improved from the version used in Paper I, and for some objects the best-fit $R_\star$ and $T_\star$ deviate slightly from Paper I. For example, HIP 42430 was fit with $R_\star$ of 1.83 $R_\odot$ and $T_\star$ of 5600 K in Paper I, but the improved fit gives $R_\star$ of 1.73 $R_\odot$ and $T_\star$ of 5800 K in Table 2. Our estimations of $R_\star$ are in good agreement with direct measurements such as those with the Very Large Telescope (VLT) interferometer as illustrated in Paper I. The accuracy of our stellar radius measurements is discussed in more detail in a separate paper (S. Kim et al. 2007, in preparation).

A single-temperature blackbody fit to the dust component yields $T_{\rm dust}$ (col. [8]) for each star, assuming blackbody radiation from dust grains in an optically thin disk. In the case of an *IRAS* detection at 60 μm, but with only upper limits at 25 and 100 μm, we set $T_{\rm dust}$ at 85 K so that the combined flux of the star and dust peaks near 60 μm. This approach leads to a conservative estimate of τ (col. [11]) ($= L_{\rm IR}/L_{\rm bol}$). Additional measurements from *Spitzer* and/or *ISO* were used to better constrain the dust temperature for stars in which such values are available in the literature or from our calculations (see § 2).

The characteristic orbital semimajor axis of dust particles, $R_{\rm dust}$, is derived from $R_{\rm dust} = (R_\star/2)(T_\star/T_{\rm dust})^2$ and listed in column (9) in AU. The corresponding angular separation (arcseconds) between dust particles and the star is indicated in column (10). The conservative nature of $R_{\rm dust}$ and the angular separation—in the sense that the actual value of $R_{\rm dust}$ at a given star may be substantially larger than the value given in column (9)—is discussed in detail in Paper I. Using a simple model of a thin dust ring (see § 5.1), dust mass (col. [12]) was estimated for 61 stars whose dust excess was detected at two or more wavelengths and whose dust radii lie between 9 and 100 AU. Table 2 lists dust mass for a total of 78 stars including 17 stars for which dust mass was obtained by direct submillimeter measurements.

Estimation of the age of a star that belongs to a known kinematic stellar group (Zuckerman & Song 2004b) is relatively straightforward. For stars not presently known to be a member of such a group, age estimation is quite difficult and requires cross-checking of several different techniques (Decin et al. 2003; Zuckerman & Song 2004b and references therein). The age estimate and age estimation methods for each star is given in columns (13) and (14), respectively. We follow the same lettering convention for each method as indicated in Paper I. A comprehensive review of different techniques of age estimation is found in Zuckerman & Song (2004b).

When available, confirmation of dust excess from MIPS and/or *ISO* measurements are indicated in column (15), and additional notes for individual objects are marked in column (16). For completeness, we repeat the notes of Table 1 from Paper I in this paper. Finally, a list of rejected sources and the reason for rejection from our survey are presented separately in Table 4.

5. DUST EVOLUTION OVER TIME

Figure 4 illustrates the temporal evolution of τ. The spectral type of each star is represented by the color of each circle, from

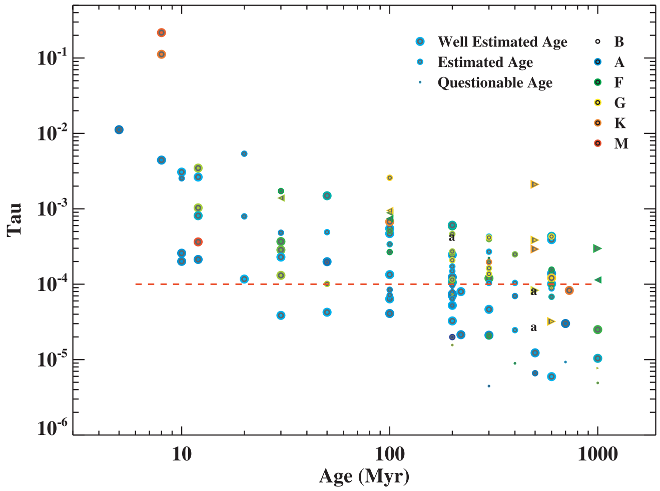

FIG. 4.—Parameter τ as a function of stellar age. The lowercase "a"s are Algol-type stars. Well-estimated ages, estimated ages, and questionable ages correspond, respectively, to zero, one, and two question marks in col. (13) of Table 2. Stars with cautions noted in Table 2 for possible contamination are not plotted in the figure.

dark blue for B-type to red for M-type. Circle size reflects the quality of our estimate of age; large, medium, and small circles depict good-, normal-, and low-quality age estimates, respectively, as given in column (13) of Table 2. The following list summarizes some characteristics indicated by the distribution of stars in Figure 4.

1. For stars with ages between ~10 Myr and 1 Gyr, the mean τ of stars with detectable excess emission declines in proportion to (age)$^{0.7}$, but with a dispersion in detected τ of a factor of ~30 at a given age.
2. The percentage of nearby stars with 60 μm excess emission detectable by *IRAS* diminishes with increasing stellar age.
3. The minimum τ is $\sim 10^{-5}$ for early-type (B, A, and F) stars and $\sim 10^{-4}$ for later types. This is due to *IRAS* sensitivity limits and the uncertainty of photospheric flux estimation.
4. At any given age, late-type stars tend to have the largest τ.

As we mentioned in § 3, no pre-2005 analysis of *IRAS* data is germane to the time evolution of fractional dust excess, τ. By contrast, three teams (Habing et al. 2001; Spangler et al. 2001; Decin et al. 2003) investigated the temporal evolution of the dust using the *ISO* database. All three studies suffer to some degree from small numbers of detected *ISO* sources, uncertain/incorrect stellar ages, or both. Decin et al. (2003) noticed that there are few young stars with $\tau < 10^{-4}$, which also appear in our Figure 4. This rarity of young, low-τ stars may be due to the fact that there are not many young early-type stars in the solar vicinity (say, $\lesssim$50 pc).

We can roughly quantify item (2) by dividing the *IRAS* stars into three age bins, (*a*) 10–50 Myr, (*b*) >50–500 Myr, and (*c*) >500–5000 Myr. We assume that, in a given volume of space near Earth, stars are uniformly distributed in age for ages up to ~1 Gyr. For older stars one first loses all main-sequence A-type stars—these evolve off the main sequence in 1–2 Gyr—followed by the loss of F-type main-sequence stars at ages between ~2 and 4 Gyr (Schaller et al. 1992).

From Figure 4, there are 26 stars in bin (*a*), 74 in bin (*b*), and 24 in bin (*c*). By our assumption of equal numbers of stars of any given age in the volume accessible to the sensitivity of *IRAS*, the age bin (*b*) contains 10 times more stars in total—with and without a dusty disk—than does bin (*a*). Since bin (*b*) in Figure 4 contains about 2.8 times the number of Vega-like stars as does bin (*a*), the probability that a star will be Vega-like is ~3.5 times greater between ages of 10 and 50 Myr than between 50 and 500 Myr.

Similarly, we can estimate the probability that a star in age bin (*c*) will be Vega-like. We ignore for just a moment the loss of A- and F-type stars in bin (*c*) as a result of evolution off the main sequence. In that case, because bin (*c*) contains 10 times more stars in total—with and without a dusty disk—than does bin (*b*) but fewer Vega-like stars (24 vs. 74), the probability that a star will be Vega-like in age bin (*b*) would be 30 times greater than in bin (*c*). However, because there is a sequential loss of A- and F-type main-sequence stars at ages > 1 Gyr, and because these spectral types dominate the *IRAS*-detected 60 μm excess stars, we estimate that if a star has an age appropriate for bin (*b*), then the probability of its being Vega-like is only ~10 times (rather than 30 times) greater than the probability of being Vega-like if its age falls in that of bin (*c*). Then the probability of any given nearby star in age bin (*a*) being Vega-like is ~35 times greater than this probability is in bin (*c*).

The preceding discussion pertains to how the probability of being Vega-like declines with age. We can estimate the absolute value of this probability in two ways. First, two stars in Table 2 are members of the Hyades (Fig. Set 2: HIP 18975 = VB 160 and HIP 20635 = VB 54), although both have cautionary notes and the 60 μm excesses cannot be regarded as definite until confirmed with additional data. *IRAS* could have detected excess 60 μm emission comparable to $\tau = 6 \times 10^{-5}$ at Hyades stars with $V \lesssim 6$, which corresponds to a mid-F-type star. According to Table 1 in Stern et al. (1995), 40 Hyades members have a *V* mag brighter than 6. Thus, at an age of 600 Myr, 5% of A- through mid-F-type stars in the Hyades are Vega-like above the 60 μm flux level accessible to *IRAS*.[6]

Field A-type stars supply a second sample to estimate the probability that a star will show the Vega phenomenon. We find, in essential agreement with some previous determinations, that *IRAS* detected 60 μm excess emission at ~20% of A-type stars with $\tau > 10^{-5}$ out to 28 pc (10 of 50 stars) and with $\tau > 4 \times 10^{-5}$ out to 40 pc (22 of 119 stars). The percentage of F-type stars that show the Vega phenomenon at comparable levels of τ appears to be noticeably smaller, but definitive statistics should wait for results from *Spitzer*.

Notwithstanding the much larger probability of a star being Vega-like at young ages, there appears to be very little distinction with age in peak τ seen in Figure 4 and noted in item (1) above. This suggests that the Vega phenomenon, at least at the higher levels of τ measured by *IRAS*, may be mostly the result of occasional large and violent collisional events rather than many small-scale, dust-producing events added together. For example, there was a very substantial and recent collisional event at the G-type main-sequence star BD +20 307, first detected by *IRAS* at 12 and 25 μm (Song et al. 2005).

Item (4) noted above might be anticipated in a collisional cascade model (cf. Dominik & Decin 2003). In such a model, collisions grind dust particles down to smaller and smaller sizes until sufficiently small particles are blown out of the system by radiation pressure from the star. Lower luminosity, later type stars will retain more small particles in orbit that in total can possess a large emitting area; thus, τ is increased. The larger τ

[6] Spangler et al. (2001) reported a 60 μm *ISO* detection of Hyades member HIP 20261, but at a flux level, 50 mJy, below the *IRAS* detection limit.

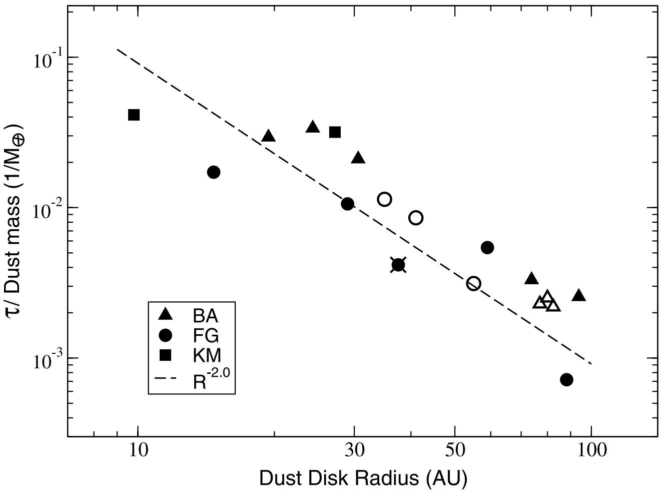

FIG. 5.—Ratio $\tau/M_{\rm dust}$ as a function of dust radius (AU). The mass $M_{\rm dust}$, given in Earth masses ($M_\oplus$), is derived from submillimeter measurements reported in the published literature. The filled and open symbols represent dust mass determinations based on submillimeter data published prior to 2006 and during 2006, respectively. The dashed line has slope, R^{-2}, but is not a formal "best fit" to the data points. See § 5.1 for further discussion. To achieve consistency among data reported in various published papers, all masses given in the plot have been normalized (by us) to have a dust opacity of 1.7 cm^2 g^{-1} at 850 μm and dust temperature as given in our Table 2. However, uncertainties in the 850 μm dust opacity caused by different grain sizes and compositions can result in the over- or underestimate of dust mass by a factor of 3 or so (e.g., Pollack et al. 1994; Beckwith et al. 2000). Meanwhile, the relative masses of the various submillimeter determinations might be better constrained than their absolute values if each star has reasonably similar dust. In the figure, the relative masses are probably trustworthy to about a factor of 2. All stars plotted have measured far-IR excess emission in at least two wavelengths. The τ for one star (HD 104860) is from *ISO*, not *IRAS*, and is marked by a cross.

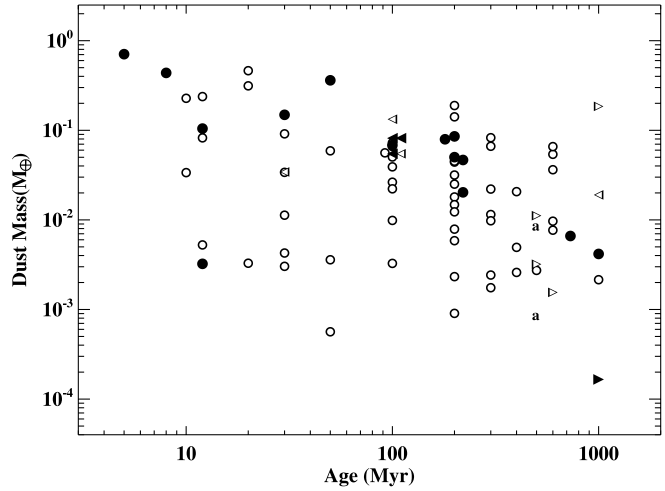

FIG. 6.—Mass $M_{\rm dust}$ as a function of stellar age. Filled symbols depict $M_{\rm dust}$ obtained from submillimeter measurements, while open symbols represent $M_{\rm dust}$ derived from Fig. 5 (see § 5.1). All stars plotted have measured far-IR excess emission in at least two wavelengths and $R_{\rm dust}$ between 9 and 100 AU. Stars with cautions noted in Table 2 for possible contamination are not plotted in the figure. Two Algol-type stars are plotted with a lowercase "a" (although their IR excess may not be due to dust particles; see § 5.2).

expected for late-type stars in a Dominik & Decin (2003) model is illustrated in their Figure 1*f*. Earlier, Song (2001) had suggested that late-type stars display larger τ than early-type stars based on the limited data available to him at that time.

5.1. *Relationship among τ, Disk Mass, Radius, and Stellar Age*

Perhaps the quantities of most interest are disk dust mass, disk radial extent, and disk evolution with time. The total mass (M) of dust in a disk may be written as

$$M = \rho N 4\pi a^3/3, \tag{7}$$

where N is the total number of grains in the disk and ρ and a are the density and radius of a typical grain, respectively. For an optically thin dusty ring of characteristic radius R,

$$\tau = N\pi a^2/4\pi R^2. \tag{8}$$

Then,

$$\tau/M \propto 1/\rho a R^2. \tag{9}$$

Thus, if characteristic grain size and density do not vary much among various optically thin dust disks, then one expects τ/M to vary as the inverse square power of the disk radius, R. Figure 5 shows this to be approximately the case for dust disks with semimajor axes between 10 and 100 AU, where we have taken τ and R from Table 2, and the disk mass from the submillimeter literature.

The significance of the filled and open symbols in Figure 5 is as follows. The figure was initially prepared containing only the filled symbols that represent dust mass determinations based on submillimeter data published prior to 2006. The dashed line was deemed a reasonable R^{-2} "fit" to these filled symbols, and we used it to derive disk dust masses for many stars in Table 2 as outlined below. Then, while the present paper was being refereed, a paper presenting measured submillimeter masses for six Table 2 stars appeared (HD 14055, 15115, 21997, 127821, 206893, and 218396; Williams & Andrews 2006). These six stars appear in our Figure 5 as open symbols, and because they lie along the dashed line, they clearly indicate the viability of our method.

While recognizing a caveat of statistics of small numbers, relative to the dashed line the early-type stars preferentially lie somewhat above the later type stars. This difference could be attributed to smaller grains around the later type stars (as discussed in § 5). However, this model requires that these grains are sufficiently small that they are unable to radiate like blackbodies at their temperature and thus, at a given distance from the star, are hotter than blackbody grains would be at that same distance.

Rather few stars appear in Figure 5 as a direct consequence of the limited number of published measurements of submillimeter fluxes for Vega-like stars. In addition, we plot only stars for which far-IR excess emission has been measured in at least two wavelengths; for such stars we can estimate $T_{\rm dust}$ and, thus, $R_{\rm dust}$.

Because τ is easier to measure (especially with *Spitzer*) than is a submillimeter flux, we use Figure 5 to derive initial estimates of dust masses for many stars listed in column (12) of Table 2. Combining *IRAS*, *ISO*, and *Spitzer* data, all stars with masses listed in Table 2 and plotted in Figure 6 have measured excess IR emission in at least two wavelengths. As mentioned in § 4 and emphasized in Paper I, the method used to calculate

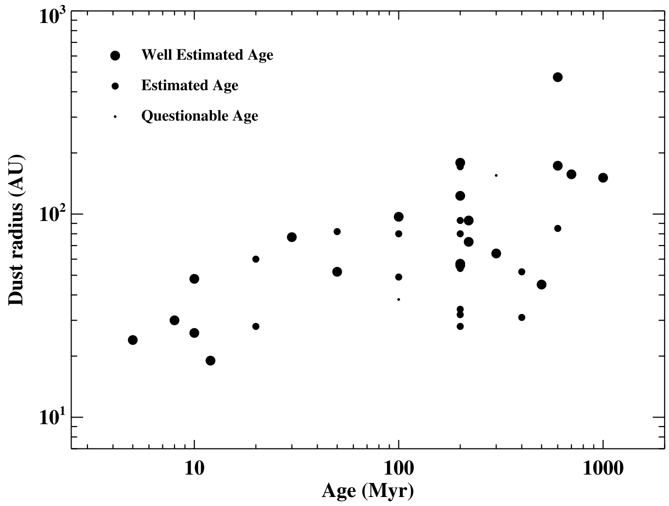

FIG. 7.—Dust radii of early-type IR excess stars (B and A) as a function of stellar age. All stars plotted have measured far-IR excess emission in at least two wavelengths. Stars with cautions noted in Table 2 for possible contamination are not plotted in the figure.

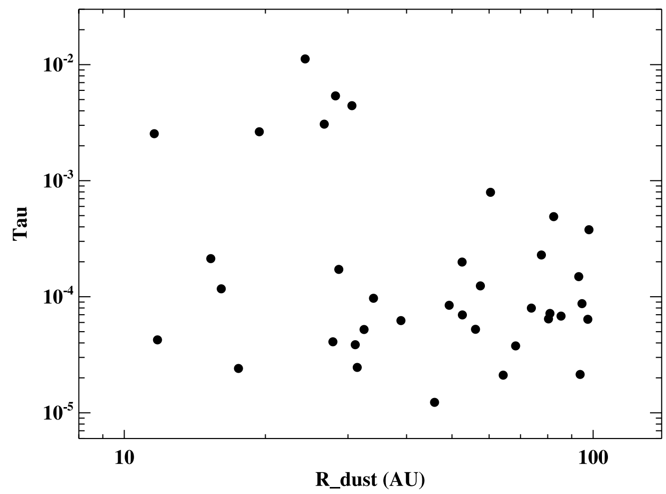

FIG. 8.—The τ of early-type IR excess stars (B and A) as a function of dust radii. All stars plotted have measured far-IR excess emission in at least two wavelengths. Stars with cautions noted in Table 2 for possible contamination are not plotted in the figure.

the values of $R_{\rm dust}$ listed in Table 2 will sometimes substantially underestimate the true $R_{\rm dust}$. Thus, the Table 2 dust mass estimates should be regarded with some caution.

The filled symbols in Figure 6 indicate a dust mass measurement at submillimeter wavelengths. We expect that stars plotted with ages $\lesssim$10 Myr still retain significant amounts of orbiting primordial dust left over from the star formation process. Thus, when considering the evolution of disk masses in dust, these stars should not be compared with the older stars whose dust is of a second generation. Figure 5 in Najita & Williams (2005), based solely on submillimeter data, is suggestive of dust mass decreasing with time. However, when stars with ages $\lesssim$10 Myr are omitted, the remaining submillimeter data are consistent with constant average dust mass at stars with ages between 30 and 1000 Myr, as suggested by our simple model from Figure 5, and the resulting open points are plotted in Figure 6.

Najita & Williams (2005) consider in some detail planet formation models of Kenyon & Bromley (2004a, 2004b). According to the discussion in Najita & Williams, in these models a wave of planet formation in the disk propagates outward, generating, as time progresses, dusty debris at successively larger characteristic radii. According to the models, for times perhaps as long as 1 Gyr, the total mass in small grains sensibly remains constant, while, in contrast, the reprocessed luminosity (i.e., τ) emitted by the collisional debris begins to decline at a much earlier time ($\lesssim$10 Myr). This is because, as the wave of planet formation moves outward, grains of a given size subtend increasingly smaller solid angles the farther they are located from the star. Comparing our results (Figs. 4 and 7) with these models, both a decrease in τ and an increase in R appear plausible between 10 and 1000 Myr.

Figure 8 is a plot of τ versus disk radius. The six stars with $\tau > 10^{-3}$ all have estimated ages of $\lesssim$20 Myr. Thus, much of their dust may be a remnant of the star formation process, rather than second generational. For the other stars, no correlation is apparent between τ and R. Although a grain of a given radius located close to a star will absorb more stellar radiation than one far away, the lifetime of close-in grains might be shorter than for distant grains, and these two effects may roughly cancel, on average.

5.2. *Algol-Type Binary Stars with Far-IR Excess Emission*

An Algol is a binary in which the less massive stellar component fills its Roche lobe and the other, which does not, is not degenerate (Batten 1989). Four stars in Table 2 are eclipsing binaries of the Algol type, including Algol A itself. HIP 76267 was long ago recognized as a 60 μm *IRAS*-excess star (Aumann 1985). The Rieke et al. (2005) *Spitzer* survey at 24 μm included three Algols. For HIP 76267, they report a just significant, 29%, excess according to their criteria (the *Spitzer* measured flux must be >1.25 times the expected photosphere to be regarded as significant). Rieke et al. also report a 7% excess at 24 μm for Algol A, although this does not meet their significance threshold of 25%. For HD 40183 their measured 24 μm flux was only 0.88 times the expected photosphere. Although the *IRAS* FSC reports detection of HD 40183 at 12, 25, and 60 μm, we see no evidence of an excess at any wavelength.

The far-IR excess emission at the four Algols might be generated by free-free and bound-free transitions in ionized gas, by cool dust, or both. The Algol-type binary stars are susceptible to emission in ionized gas because a small H II region is created around the primary star by material transferred from the secondary star. We first consider far-IR emission in an ionized gas disk orbiting a late B-type primary in Algols listed in Table 3. We assume an electron density $n_e = 10^{10}$ cm^{-3} and a disk radius $r = 10^{12}$ cm (Peters 1989; Guinan 1989). Code et al. (1976) give the flux between 0 and 1100 Å received at Earth for the B7 star α Leo. This translates to $\sim 2\times 10^{44}$ photons s^{-1} emitted by α Leo and capable of ionizing hydrogen. The excitation parameter (E), i.e., the number of photons per second required to maintain an H II region, is

$$E = (4\pi/3) r^3 n_e^2 \alpha_B \qquad (10)$$

(Osterbrock 1974, p. 21 and 79). With $\alpha_B = 2\times 10^{13}$ cm^3 s^{-1} at 10,000 K and $E = 2\times 10^{44}$ ionizing photons s^{-1}, an H II region with $n_e = 10^{10}$ cm^{-3} and $r = 10^{12}$ cm can be supported.

Considering the four Algols with SEDs displayed in Figure 9, we assume a characteristic distance of 30 pc and a characteristic excess flux at 60 μm equal to 0.4 Jy. The orbiting ionized disk described in the preceding paragraph would have a 60 μm

TABLE 3
ALGOLS FROM *IRAS* AND *Spitzer*

			Rieke et al. (2005)			
HIP	HD	Other	Observed?	Excess?	This Paper Excess?	Triple System?
14576	19356	Algol A	Yes	1.07 (no)	Marginal?	Yes
21604	29365	HU Tau	No		Strong	?
28360	40183	β Aur	Yes	0.88 (no)	Nothing	?
73473	132742	δ Lib	No		2 wavelengths	Yes
76267	139006	α CrB	Yes	1.29 (yes)	2 wavelengths	?

optical depth ~0.2 (Osterbrock 1974, p. 21 and 79) and could account for this excess flux. Thus, it is plausible that ionized gas, rather than dust, could generate the excess far-IR emission in some or even all Algols.

Cool dust might also be present in some of these systems. The fact that Algol itself and HIP 73473 are both triple systems (Worek 2001) may supply a clue as to why cool dust is present at all. In addition to the characteristic mass transfer between primary and secondary, analysis indicates mass is also lost from Algol systems (Batten 1989). If a tertiary component is present, then the system could be analogous in essential respects to binary post–asymptotic giant branch (post-AGB) stars, many of which are known to be orbited by a dusty circumbinary disk (e.g., Waters et al. 1991). That is, the central object (a single star in the case of the post-AGB stars and a binary in the case of Algols) ejects mass, some of which is captured into a dusty surrounding disk by the gravity of an orbiting companion.

While such a model might apply to Algol A and to HIP 73473, it need not necessarily apply to other Algols with far-IR excess emission. One obvious test would be a search for evidence of a third star in the HIP 21604 and HIP 76267 systems.

6. SUMMARY AND CONCLUSIONS

The 1983 all-sky *IRAS* far-IR survey yielded a wealth of information about the properties of cool dust in orbit around main-sequence stars. However, notwithstanding decades of ground- and space-based follow-up projects including *ISO*, as of 2004 when we began the research reported here, in our opinion, a consistent, convincing evolutionary picture of these dusty stars had not been published. In particular, while various researchers had cross-correlated various stellar catalogs against the *IRAS* catalog, none had used the *Hipparcos* catalog. Stellar distances and proper motions provided by the *Hipparcos* and Tycho catalogs yield information useful for establishing ages of

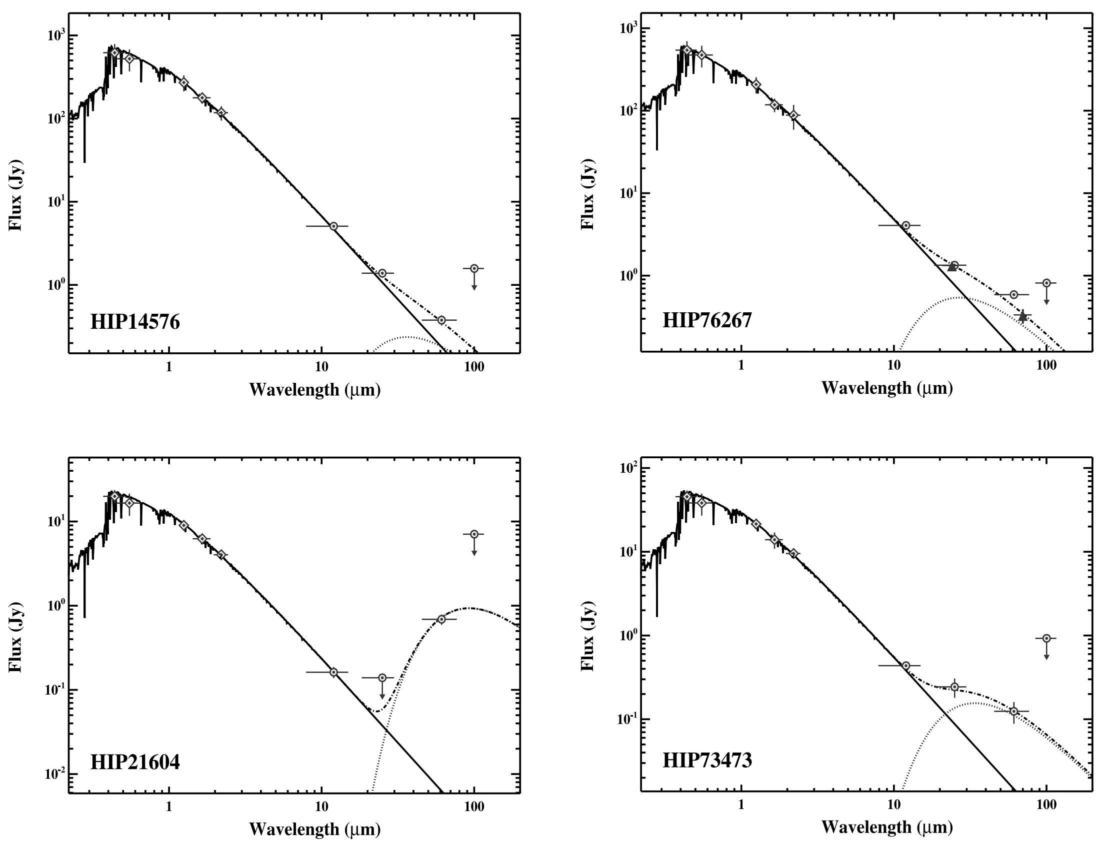

Fig. 9.—SEDs of Algol-type stars. For HIP 76267 the triangle data points at 24 and 70 μm are from Rieke et al. (2005). Fitting parameters (e.g., $R_\star$, $T_\star$, $R_{\rm dust}$, $T_{\rm dust}$) of each star are given in Table 2. However, the far-IR emission might be generated by ionized gas (see § 5.2).

dusty stars; reliable ages are essential if correct evolutionary sequences are to be deduced. In addition, as a consequence of the rather large *IRAS* beam size and inadequate attention to elimination of background confusion, some previous stellar studies with *IRAS* have suffered from the inclusion of false-positive far-IR-excess stars.

In the research reported here we have taken special pains to deduce stellar ages and to eliminate false positives. Just as it is possible to deduce many properties of stellar clusters and associations even though some stars are mistakenly included as members, we trust that our Table 2 *IRAS* sample is clean enough that our conclusions will stand the test of time. Nonetheless, because ages of nearby field stars are notoriously difficult to estimate accurately and because of limitations with the *IRAS* database, we recognize that some entries in the tables and figures presented in this paper will be in error.

IRAS was most effective for the study of luminous B- and A-type main-sequence stars. In agreement with some earlier studies, we find that *IRAS* detected excess emission at 60 μm from about 20% of nearby A-type stars. This percentage will certainly rise as the A stars are examined with far-IR photometers more sensitive than those aboard *IRAS*. In particular, we find that about 10% of stars of various spectral classes are revealed to display far-IR dust emission at brightness levels between *IRAS* and *Spitzer* sensitivities. Although this 10% subsumes stellar age, spectral types, and distance from Earth, and thus is potentially subject to selection effects, it is consistent with the well-defined TW Hydra association sample of Low et al. (2005). Using heterogeneous samples, Smith et al. (2006) and Bryden et al. (2006) also reported about 10% of stars show dust excess in the MIPS 70 μm band, but below *IRAS* sensitivity.

From their analysis of *ISO* data sets, especially the volume-limited sample of Habing et al. (2001), Decin et al. (2003) deduced that the percentage of stars with detectable 60 μm emission diminishes with age. However, the small data set of Habing et al. (2001) and difficulties with estimating stellar age precluded a meaningful quantitative result in our opinion. With our larger and more robust database we can derive that the probability of 60 μm excess emission detectable with the sensitivity of *IRAS* is about 35 times larger for A- and F-type stars with ages in the range 10–50 Myr compared to such stars with ages >500 Myr in the volume within 120 pc of Earth.

While it is generally agreed that measurements at submillimeter wavelengths are best for the derivation of dust masses, by means of a simple model that relates submillimeter and far-IR fluxes, we are able to derive dust masses for numerous stars that lack submillimeter data. These masses lie in the range between 0.0005 and 0.5 $M_\oplus$. For stars with ages between 30 and 1000 Myr, these dust masses appear to depend little, if at all, on age. Based on Figure 5 and as described in § 5.1, our model indicates that far-IR data can be used, quite reliably, to predict a submillimeter flux and, thus, a disk dust mass. As a consequence, disk dust masses can generally be derived based solely on *Spitzer* data provided that excess flux is measured at two or more well-separated wavelengths with MIPS and/or the Infrared Spectrograph (IRS).

Four Algol binary stars appear to display excess emission at 60 μm wavelength, although the existence of the excess is perhaps not compelling in all cases. We considered models in which the emission is generated by free-free and bound-free emission in orbiting ionized gas or by orbiting dust particles, dust perhaps associated with a tertiary (third) stellar component. Future studies will be required to clarify the dominant physical mechanism(s) involved.

Additional results of our study include (1) peak τ ($\sim10^{-3}$) does not vary much at all ages later than $\sim$10 Myr; this might be because occasional catastrophic dust-generating events can occur at any age. (2) The spread of measured τ at ages $\sim$10 Myr is about a factor of 10, increasing to about 100 at later ages; given the measured peak τ (item 1) and *IRAS* threshold ($\sim10^{-5}$), the measured spread of τ cannot be greater than 100. (3) At any given age late-type stars tend to have the largest τ. (4) For stars with ages between 10 and 1000 Myr, the mean τ of stars with *IRAS* detectable far-IR excess emission declines in proportion to (age)$^{0.7}$. (5) For early-type stars between ages of $\sim$10 and 100 Myr, the typical radius of a dusty debris disk appears to be smaller than for stars with ages between 100 Myr and 1 Gyr. (6) The very largest taus ($>10^{-3}$) are associated only with disks that have relatively small radii. (7) *IRAS* detected excess 60 μm emission from $\sim$20% of nearby A-type stars. (8) Four Algol-type eclipsing binaries, including Algol A itself, display 60 μm emission, generated by free-free and bound-free transitions in ionized gas, by dust grains, or by both. (9) Gl 803 (AU Mic, 12 Myr old) is the only M-type, non–T Tauri, *Hipparcos* dwarf star to display 60 μm excess emission in the *IRAS* Catalogs.

We thank the referee for his/her constructive comments that helped to improve this paper. We also thank Travis Barman for providing a customized set of Next Gen. Phoenix models of stellar atmospheres and M. Jura for helpful comments. This research has made use of the VizieR catalogue access tool, CDS, Strasbourg, France and of data products from 2MASS (the latter is a joint project of the University of Massachusetts and the Infrared Processing and Analysis Center/California Institute of Technology, funded by the National Aeronautics and Space Administration and the National Science Foundation). We acknowledge a NASA grant NAG-13067 for financial support.

APPENDIX

REJECTED SOURCES

The list of rejected sources can be found in Table 4.

TABLE 4

List of Rejected Sources

HIP	HD	*IRAS* Source	Contamination Source	Additional Data Source	Reason for Rejection[a]
1468	1407	F00157+1907	UGC 00169	NED	1
2021	2151	F00235−7731			2
8102[b]	10700	F01416−1611		MIPS	3
8796	11443	F01502+2919			2
8817	...	F01506+2312	2MASX J01532347+2327067	NED	1
9236	12311	F01572−6148			2
12843	17206	F02427−1846		MIPS	3
13847	18622	F02563−4030			2
14897	20010	F03095+1351			2
15197	20320	F03134−0900			2
16276	20110	F03190+8352	HIP 16267		4
17378	23249	F03408−0955			2
17439	23484	F03423−3826		*ISO*	5
17531	23338	03421+2418			5, 6
17573	23408	F03428+2412	NGC 1432	NED	1
17579	23432	03429+2423			5, 6
17608	23480	F03433+2347			5, 6
17921	23950	F03469+2205			5, 6
21010	28447	F04273+2800	2MASX J04302705+2807071	NED	7
22449	30652	F04471+0652			2
23818	33095	F05049−1927			1
25110	33564	F05142+7911	IRAS F05142+7911	MIPS	1
25732	36150	05271−0050			5
27100	39014	F05446−6545			5
28360	40183	F05558+4456			2
30252	44958	F06207−5112			8
32277	...	F06407+4040	HIP 32275		4
32349	48915	06429−1639			2
32435	53842	F06539−8355		MIPS	9
34473	55864	F07091−7024			2
35457	56099	F07149+5913		MIPS	9
35789	58853	F07225−6432		IRAS F07225−6432	1
37279	61421	F07366+0520		MIPS	2
40167	68255	F08093+1747			10
42913	74956	09433−5431		MIPS	3
43100	74738	F08436+2856	HIP 43103		4
44923	78702	F09067−1807		MIPS	5
44915	78752	F09068−2844			5
45238	80007	F09126−6930			2
46853	82328	F09294+5154			2
46984	82821	F09319+0346	2MASX J09343627+0332421	NED	1
49641	87887	F10053−0007		MIPS	3
49669	87901	F10057+1212			2
54835	97455	F11107+5541	SBS 1110+556	NED	1
57583	...	F11457−2150			11
57757	102870	F11481+0202			2
57759	102902	F11482−3252	Unknown galaxy	NED	12
58001	103287	F15512+5358			2
58364	103913	11554+2524		NED	1
59307	105686	F12074−3425	GdF J1209598−344142	NED	1
60112	107228	F12171+0549	NGC 4266	NED	1
60902	108653	F12263+0126	SDSS J122856.95+010907.4	NED	1
61932	110304	F12387−4841			2
61941	110379	F12390−0110			2
61947	...	F12394+4319	2MASX J12414864+4302494	NED	1
62956	112185	F12518+5613			2
63973	113767	13036−4924	NGC 4945A	NED	1
65109	115892	F13177−3627		MIPS	2
65378	116656	F13219+5511			2
66249	118098	F13321−0020		*ISO*	2
67927	121370	F13522+1838			2
68160	121812	F13549+2336			6
68380	122106	F13571−0318	APMUKS(BJ) B135713.55−031828.8	NED	1
70497	126660	F14235+5204			2

TABLE 4—*Continued*

HIP	HD	*IRAS* Source	Contamination Source	Additional Data Source	Reason for Rejection[a]
72339	130322	F14449−0004	APMUKS(BJ) B144458.55−000415.4	NED	1
72659	131156	F14491+1918			2
75039	136580	F15182+4109	2MASX J15200834+4059114	NED	1
75118	136407	F15182−1522		MIPS	3
76641	139907	F15374+4401	UGC 09959	NED	1
77634	141556	15477−3328			6
78072	142860	F15541+1548		MIPS	2
78527	144284	F16009+5841			2
78594	143840	F16001−0440		MIPS	10
79807	147094	F16159+5229	2MASX J16171300+5222153	NED	1
81693	150680	F16393+3141			2
83137	153377	F16567−0136		MIPS	3
83343	...	F16599+2300			13
84696	156635	F17162−0245			1
85104	...	F17223+4811			9
85576	158373	F17265−0957		*ISO*	6
85790	159139	17299+2826	CGCG 170−036	NED	1
86032	159561	F17326+1235			2
86974	161797	F17444+2744			2
87815	164330	F17559+6236		*ISO*	6
89937	170153	F18220+7242			2
92683	174966	18505+0141			14
93371	176270	F18576−3708	IC 4812	NED	1
93449	...	F18585−3701	NGC 6729	NED	1
98025	189207	F19544+6227		MIPS	3
98433	189478	19575+0647			6
99240	190248	F20039−6619			2
104206	199391	F20593−8053		MIPS	3
105090	202560	F21141−3904		MIPS	2
105858	203608	F21223−6535		MIPS	2
106368	204942	F21297−2422	APMUKS(BJ) B212943.47−242303.3	NED	1
107556	207098	F21442−1621			2
108594	...	F21563−6220	APMUKS(BJ) B215622.59−622020.9	NED	1
108870	209100	F21598−5700		MIPS	2
111544	214168	F22335+3921	HIP 111546		5
111558	...	F22330−5154	ESO 238-IG 019	NED	1
114996	219571	F23145−5830		*ISO*	2
118182	...	F23558+5106	HIP 118188		5
118268	224617	F23567+0634			6

NOTE.—Unless already confirmed by additional instruments, those objects rejected because of possible cirrus contamination need confirmation from *Spitzer* MIPS 70 μm measurement.

[a] 1. There exists a nearby extended source within 3 σ *IRAS* positional error ellipse.
2. SED shows that *IRAS* 60 or MIPS 70 μm detection falls on the stellar photosphere.
3. No source was detected at the expected stellar position in MIPS 70 μm image.
4. There exists a second bright star within 3 σ *IRAS* positional error ellipse.
5. *IRAS* 60 μm excess is likely caused by cirrus contamination.
6. This star, a member of the Pleiades cluster, is likely contaminated by cirrus (Kalas et al. 2002).
7. *IRAS* SCANPI shows 1′ offset in in-scan direction where the listed galaxy is located.
8. The 3 σ *IRAS* positional error ellipse does not include the target star.
9. Moór et al. (2006) rejected this star based on their *Spitzer* MIPS observation.
10. Infrared excess had $<2.5\ \sigma$ detection at *IRAS* 60 μm band (see § 2 for the definition of σ).
11. *IRAS* FSC long format indicates a large offset between 60 and 12 μm positions.
12. *IRAS* SCANPI shows 30″ offset in the in-scan direction where the listed galaxy is located.
13. *Spitzer* MIPS 70 μm image shows extended emission.
14. There exists a huge background galaxy behind this star.

[b] Both *IRAS* and *ISO* reported excess emission at 60 μm, and Greaves et al. (2004) reported excess emission at 850 μm. However, *Spitzer* MIPS observations show a stellar photosphere detection at 70 μm.

REFERENCES

Aumann, H. H. 1985, PASP, 97, 885
Aumann, H. H., et al. 1984, ApJ, 278, L23
Backman, D. E., & Paresce, F. 1993, in Protostars and Planets III, ed. V. Mannings, A. P. Boss, & S. S. Russell (Tucson: Univ. Arizona Press), 1253
Batten, A. H. 1989, in Algols, ed. A. H. Batten (Dordrecht: Kluwer), 1
Beckwith, S. V. W., Henning, T., & Nakagawa, Y. 2000, in Protostars and Planets IV, ed. V. Mannings, A. P. Boss, & S. S. Russell (Tuscon: Univ. Arizona Press), 533
Beichman, C. A., et al. 2005, ApJ, 622, 1160
Bessell, M. 2000, PASP, 112, 961

Bryden, G., et al. 2006, ApJ, 636, 1098
Chen, C. H., et al. 2005, ApJ, 634, 1372
Code, A. D., Bless, R. C., Davis, J., & Brown, R. H. 1976, ApJ, 203, 417
Cox, A. N., ed. 2000, Allen's Astrophysical Quantities (New York: AIP)
Decin, G., Dominik, C., Waters, L. B. F. M., & Waelkens, C. 2003, ApJ, 598, 636
Dominik, C., & Decin, G. 2003, ApJ, 598, 626
Guinan, E. F. 1989, in Algols, ed. A. H. Batten (Dordrecht: Kluwer), 35
Habing, H. J., et al. 2001, A&A, 365, 545
Hauschildt, P. H., Allard, F., & Baron, E. 1999, ApJ, 512, 377
Jura, M., et al. 2004, ApJS, 154, 453
Kalas, P., Graham, J. R., Beckwith, S. V. W., Jewitt, D. C., & Lloyd, J. P. 2002, ApJ, 567, 999
Kenyon, S. J., & Bromley, B. C. 2004a, AJ, 127, 513
———. 2004b, ApJ, 602, L133
Kim, J., et al. 2005, ApJ, 632, 659
Kouwenhoven, M. B. N., Brown, A. G. A., Zinnecker, H., Kaper, L., & Portegies Zwart, S. F. 2005, A&A, 430, 137
Lagrange, A. M., Backman, D. E., & Artymowicz, P. 2000, in Protostars and Planets IV, ed. V. Mannings, A. P. Boss, & S. S. Russell (Tucson: Univ. Arizona Press), 639
Low, F. J., Smith, P. S., Werner, M., Chen, C., Krause, V., Jura, M., & Hines, D. C. 2005, ApJ, 631, 1170
Lowrance, P. J., et al. 2000, ApJ, 541, 390
Manoj, P., & Bhatt, H. C. 2005, A&A, 429, 525
Meyer, M. R., et al. 2004, ApJS, 154, 422
Moór, A., Abraham, P., Derekas, A., Kiss, Cs., Kiss, L. L., Apai, D., Grady, C., & Henning, Th. 2006, ApJ, 644, 525
Najita, J., & Williams, J. P. 2005, ApJ, 635, 625
Odenwald, S. F. 1986, ApJ, 307, 711
Osterbrock, D. E. 1974, Astrophysics of Gaseous Nebulae (San Francisco: W. H. Freeman)
Peters, G. J. 1989, in Algols, ed. A. H. Batten (Dordrecht: Kluwer), 9
Plavchan, P., Jura, M., & Lipscy, S. J. 2005, ApJ, 631, 1161
Pollack, J. B., Hollenback, D., Beckwith, S., Simonelli, D. P., Roush, T., & Fong, W. 1994, ApJ, 421, 615
Rieke, G. H., et al. 2005, ApJ, 620, 1010
Schaller, G., Schaerer, D., Meynet, G., & Maeder, A. 1992, A&AS, 96, 269
Silverstone, M. 2000, Ph.D. thesis, Univ. California, Los Angeles
Smith, P. S., Hines, D. C., Low, F. J., Gehrz, R. D., Polomski, E. F., & Woodward, C. E. 2006, ApJ, 644, L125
Song, I. 2001, in ASP Conf. Ser. 244, Young Stars Near Earth: Progress and Prospects, ed. R. Jayawardhana & T. Greene (San Francisco: ASP), 221
Song, I., Bessell, M. S., & Zuckerman, B. 2002a, A&A, 385, 862
Song, I., Caillault, J.-P., Barrado y Navascues, D., & Stauffer, J. R. 2000, ApJ, 533, L41
Song, I., Weinberger, A. J., Becklin, E. E., Zuckerman, B., & Chen, C. 2002b, AJ, 124, 514
Song, I., Zuckerman, B., & Bessell, M. S. 2003, ApJ, 599, 342
Song, I., Zuckerman, B., Weinberger, A. J., & Becklin, E. E. 2005, Nature, 436, 363
Spangler, C., Sargent, A. I., Silverstone, M. D., Becklin, E. E., & Zuckerman, B. 2001, ApJ, 555, 932
Stauffer, J. R., et al. 2005, AJ, 130, 1834
Stern, R. A., Schmitt, J. H. M. M., & Kahabka, P. T. 1995, ApJ, 448, 683
Waters, L. B. F. M., Trams, N. R., & Waelkens, C. 1991, in The Infrared Spectral Region of Stars, ed. C. Jaschek & Y. Andrillat (Cambridge: Cambridge Univ. Press), 40
Williams, J. P., & Andrews, S. M. 2006, ApJ, 653, 1480
Worek, T. F. 2001, PASP, 113, 964
Zuckerman, B. 2001, ARA&A, 39, 549
Zuckerman, B., Forveille, T., & Kastner, J. H. 1995a, Nature, 373, 494
Zuckerman, B., Kim, S. S., & Liu, T. 1995b, ApJ, 446, L79
Zuckerman, B., & Song, I. 2004a, ApJ, 603, 738 (Paper I)
———. 2004b, ARA&A, 42, 685
Zuckerman, B., Song, I., Bessell, M. S., & Webb, R. A. 2001a, ApJ, 562, L87
Zuckerman, B., Song, I., & Webb, R. A. 2001b, ApJ, 559, 388
Zuckerman, B., & Webb, R. A. 2000, ApJ, 535, 959